Supplement of Atmos. Meas. Tech., 15, 4001–4022, 2022
https://doi.org/10.5194/amt-15-4001-2022-supplement

Atmospheric Measurement Techniques
Open Access
EGU

Supplement of

Testing the efficacy of atmospheric boundary layer height detection algorithms using uncrewed aircraft system data from MOSAiC

Gina Jozef et al.

Correspondence to: Gina Jozef (gina.jozef@colorado.edu)

Supplementary Figures

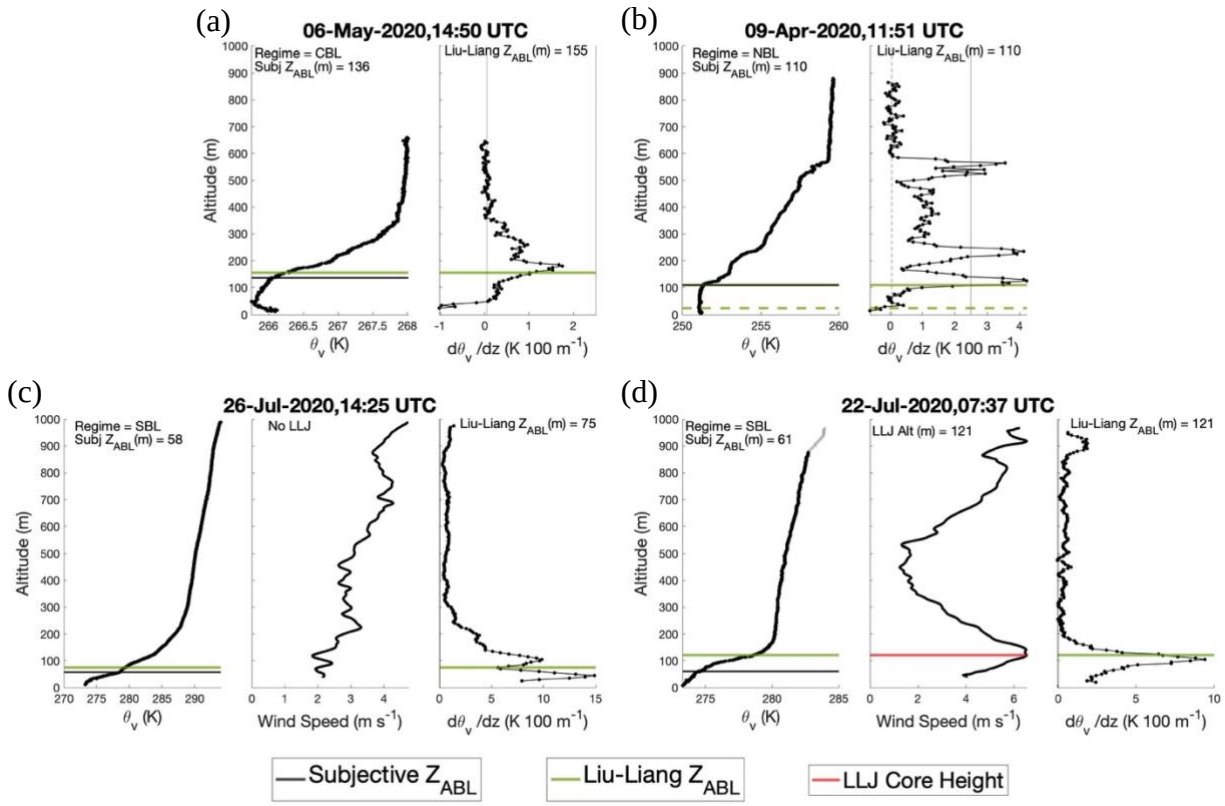

Figure S1: Examples of Z_{ABL} identification using the Liu-Liang method applied to **(a)** a CBL case, **(b)** an NBL case, and **(c-d)** SBL cases. For each of the above cases, the θ_v profile is plotted in the left panel, which includes the stability regime (written), subjective Z_{ABL} (written and marked with a horizontal black line) and Liu-Liang Z_{ABL} (marked with a horizontal green line). For each case, the $d\theta_v/dz$ profile is plotted on the right panel, which includes the Z_{ABL} from the Liu-Liang method (written and marked with a horizontal green line). For the SBL cases, wind speed is also plotted in the middle panel, which includes LLJ height if one exists (marked and written). For the CBL case **(a)**, a thin vertical black line at $d\theta_v/dz$ = 0.05 K 100 m^{-1} is plotted on the right panel. For the NBL case **(b)**, a thin vertical black line at $d\theta_v/dz$ = 2.5 K 100 m^{-1} is plotted on the right panel. Additionally, a dashed vertical black line using the original Liu-Liang threshold value of $d\theta_v/dz$ = 0.05 K 100 m^{-1} is plotted on the right panel, as well as a dashed green line at the Z_{ABL} associated with using this threshold on both panels. For both SBL cases, a thin vertical black line at $d\theta_v/dz$ = 0.05 K 100 m^{-1} is plotted on the right panel. For the first SBL case **(c)**, Z_{ABL} found by the Liu-Liang methods is determined using the buoyancy forcing criteria. For the second SBL case **(d)**, Z_{ABL} found by the Liu-Liang methods is determined as the altitude of the LLJ core.

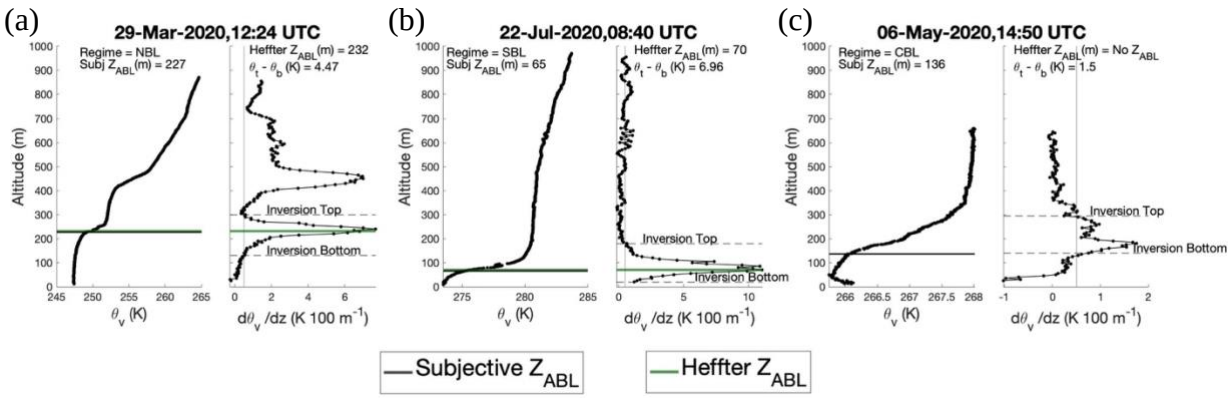

Figure S2: Examples of Z_{ABL} identification using the Heffter method applied to **(a)** an NBL case, **(b)** an SBL case, and **(c)** a CBL case. For each of the above cases, the θ_v profile is plotted in the left panel, which includes the stability regime (written), subjective Z_{ABL} (written and marked with a horizontal black line) and Heffter Z_{ABL} (marked with a horizontal green line). For each case, the $d\theta_v/dz$ profile is plotted on the right panel, which includes Z_{ABL} from the Heffter method (written and marked with a horizontal green line), θ_v difference across the θ_v inversion (written), a thin vertical black line plotted at $d\theta_v/dz$ = 0.5 K 100 m^{-1}, and the top and bottom of the θ_v inversion (marked with dashed horizontal black lines). No Heffter Z_{ABL} is found for the CBL case since the θ_v difference across the θ_v inversion is less than 2 K.

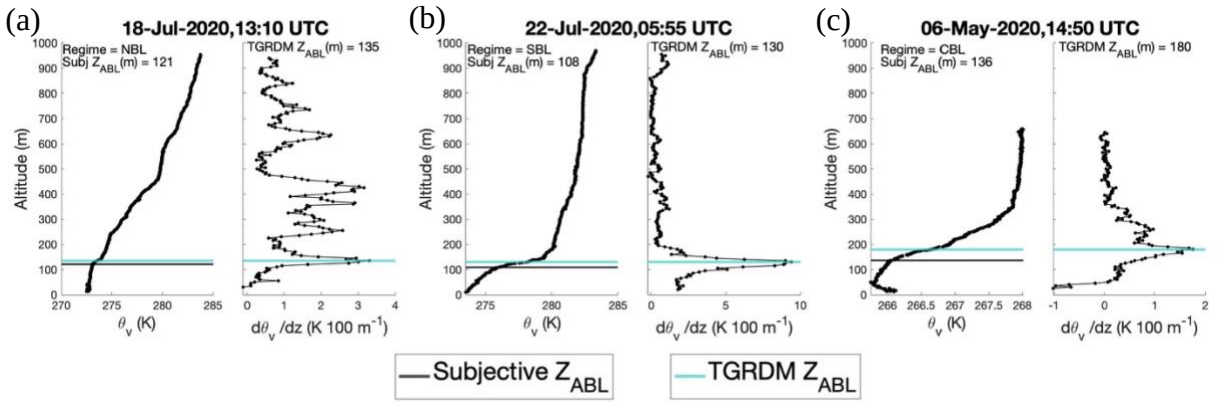

Figure S3: Examples of Z_{ABL} identification using the TGRDM method applied to **(a)** a NBL case, **(b)** an SBL case, and **(c)** a CBL case. For each of the above cases, the θ_v profile is plotted in the left panel, which includes the stability regime (written), subjective Z_{ABL} (written and marked with a horizontal black line) and TGRDM Z_{ABL} (marked with a horizontal blue line). For each case, the $d\theta_v/dz$ profile is plotted on the right panel, which includes Z_{ABL} from the TGRDM method (written and marked with a horizontal blue line).

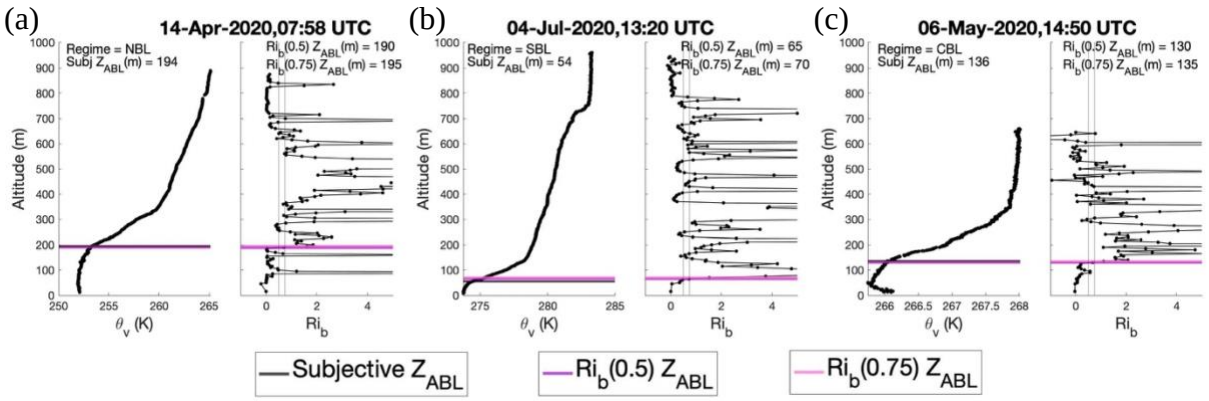

Figure S4: Examples of Z_{ABL} identification using the Ri_b method applied to **(a)** an NBL case, **(b)** an SBL case, and **(c)** a CBL case. For each of the above cases, the θ_v profile is plotted in the left panel, which includes the stability regime (written), subjective Z_{ABL} (written and marked with a horizontal black line) and Ri_b Z_{ABL} (marked with horizontal purple and pink lines). For each case, the Ri_b profile is plotted on the right panel, which includes Z_{ABL} from the Ri_b method with each threshold value (written and marked with horizontal purple and pink lines), and thin vertical black lines plotted at $Ri_b = 0.5$ and $Ri_b = 0.75$.

Figures S5-S69: Examples of Z_{ABL} identification for all DH2 flights (represented by solid lines) used in the current study and the corresponding radiosonde profiles (represented by dashed lines). Panel 1: θ_v profile from the DH2. Panel 2: θ_v profile from the radiosonde. Panel 3: Ri_b profiles from the DH2 (solid black) and the radiosonde (dashed grey). Panel 4: $d\theta_v/dz$ profiles from the DH2 (solid black) and the radiosonde (dashed grey). Panel 5: wind speed profiles from the DH2 (solid black) and radiosonde (dashed grey). The legend below indicates the Z_{ABL} detection method associated with each horizontal line in Figures S5-S69. LLJ core is not in itself a Z_{ABL} detection method, but plays into the Liu-Liang method, so it is included. Each Z_{ABL} is written on the corresponding platform's θ_v profile. 'No Z_{ABL}' is written if the method fails to identify a Z_{ABL}.

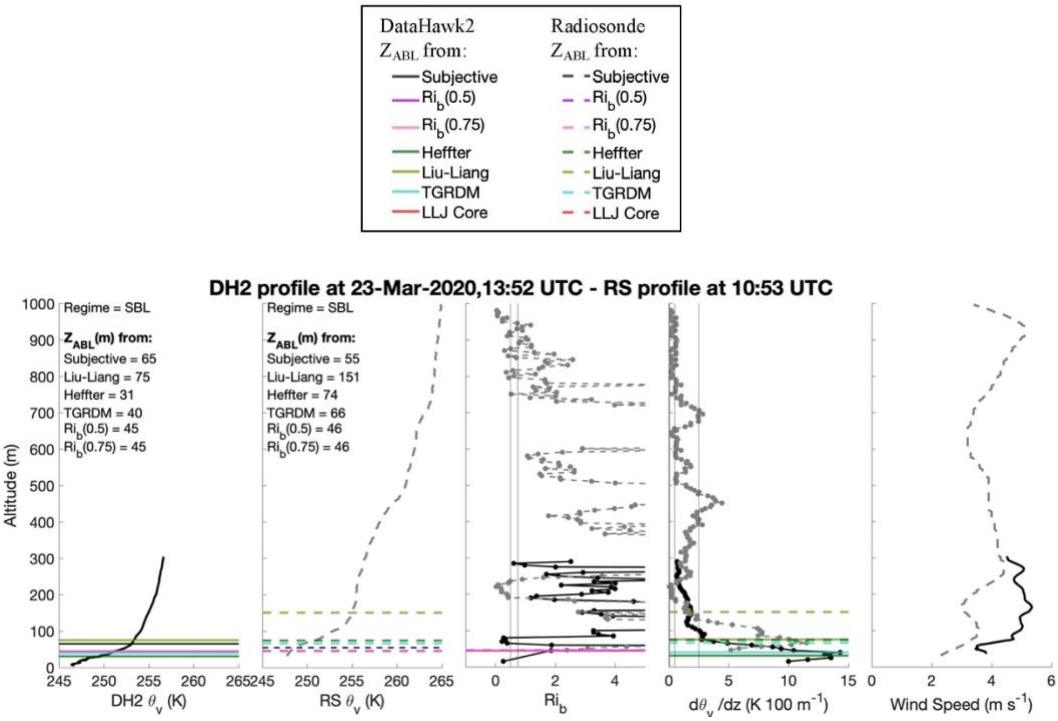

Figure S5: Z_{ABL} identification for DH2 flight on 23 March at 13:52 UTC and radiosonde profile at 10:53 UTC.

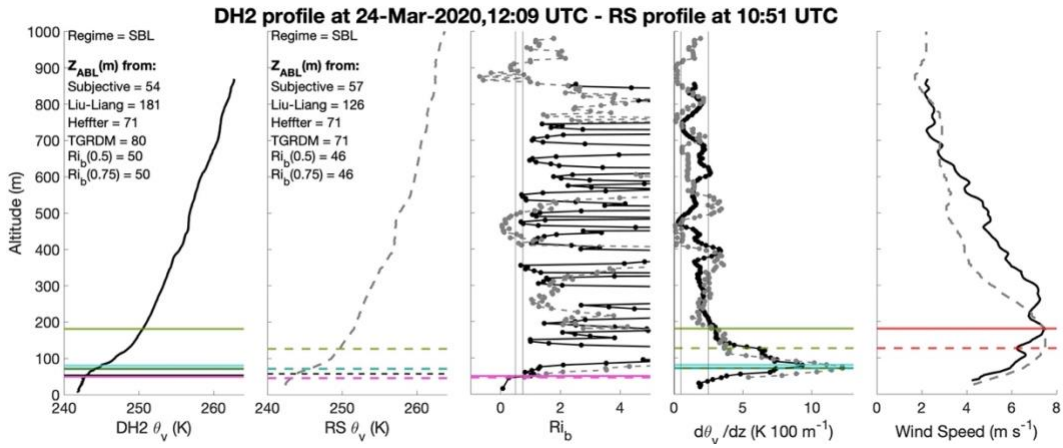

Figure S6: Z_{ABL} identification for DH2 flight on 24 March at 12:09 UTC and radiosonde profile at 10:51 UTC.

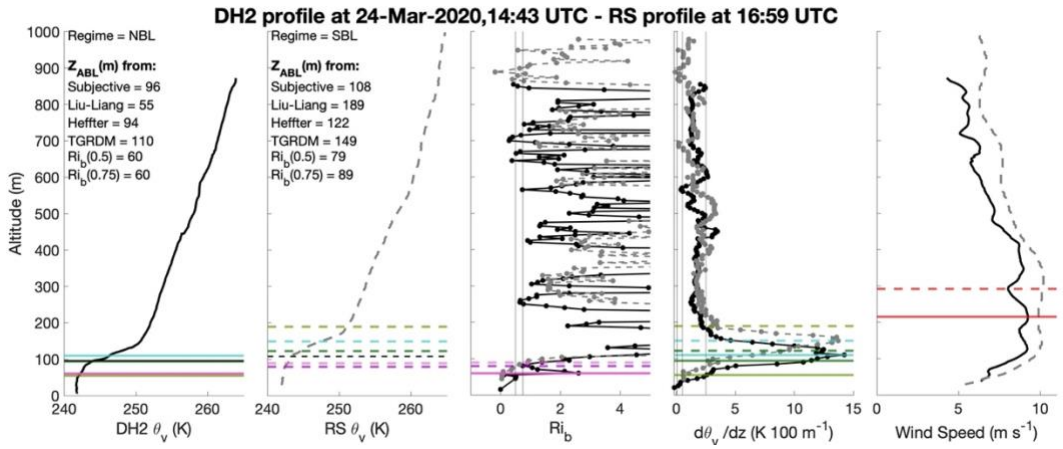

Figure S7: Z_{ABL} identification for DH2 flight on 24 March at 14:43 UTC and radiosonde profile at 16:59 UTC.

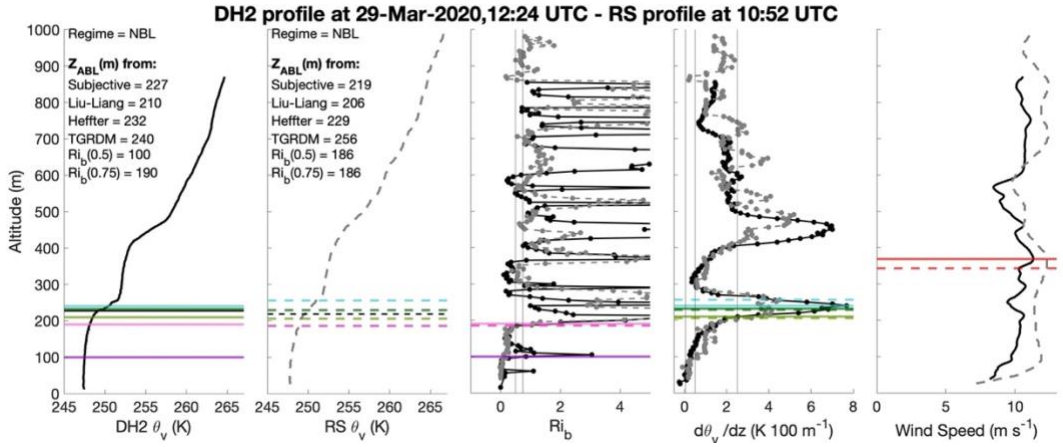

Figure S8: Z_{ABL} identification for DH2 flight on 29 March at 12:24 UTC and radiosonde profile at 10:52 UTC.

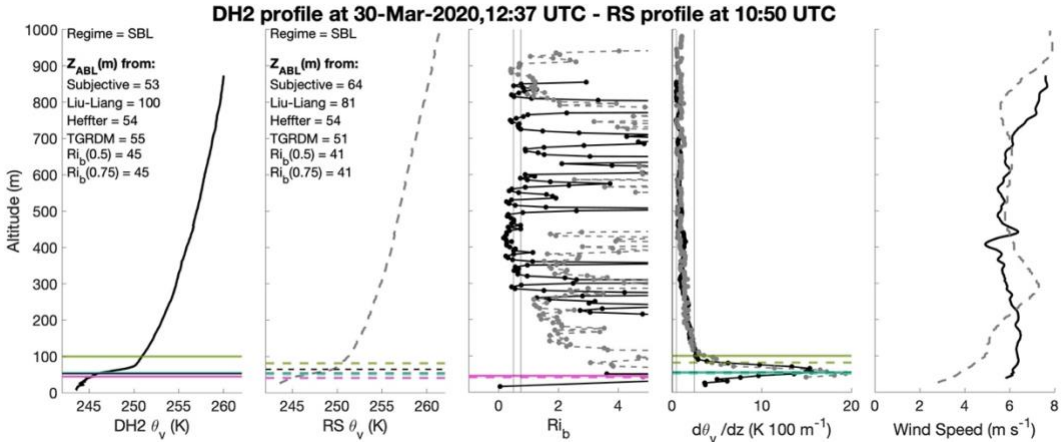

Figure S9: Z_{ABL} identification for DH2 flight on 30 March at 12:37 UTC and radiosonde profile at 10:50 UTC.

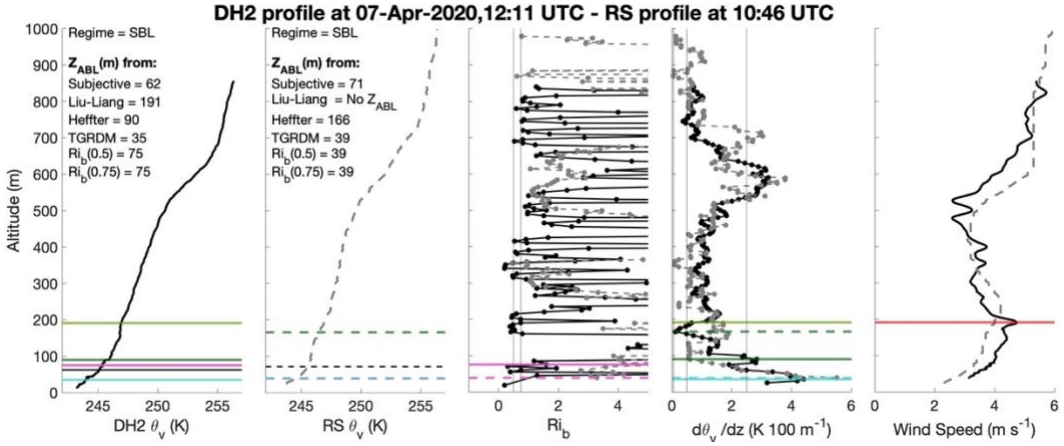

Figure S10: Z_{ABL} identification for DH2 flight on 7 April at 12:11 UTC and radiosonde profile at 10:46 UTC.

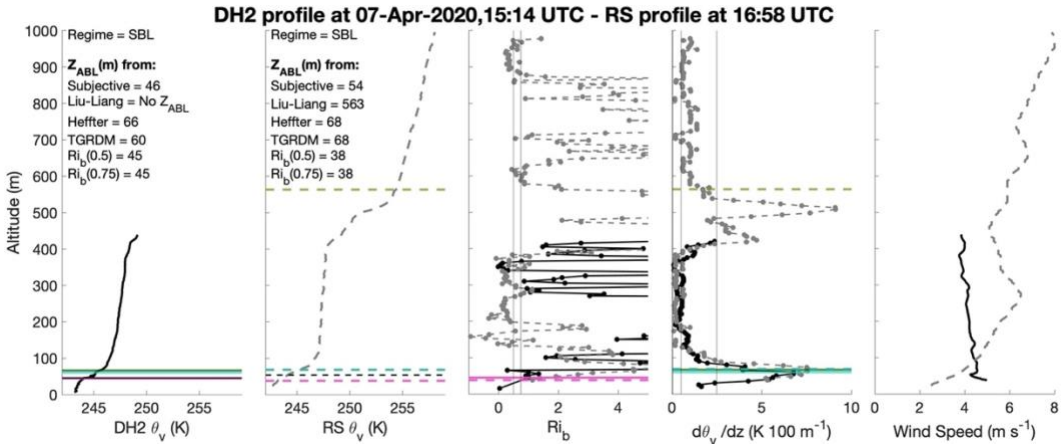

60

Figure S11: Z_{ABL} identification for DH2 flight on 7 April at 15:14 UTC and radiosonde profile at 16:58 UTC.

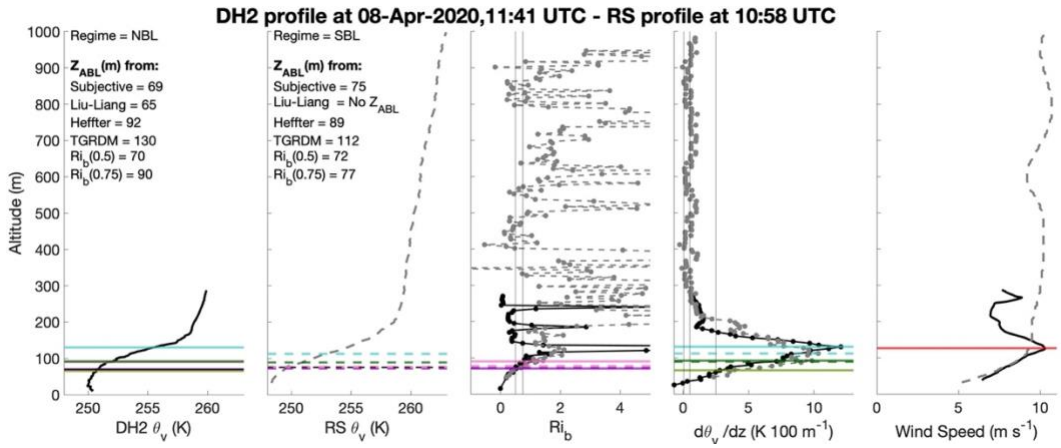

Figure S12: Z_{ABL} identification for DH2 flight on 8 April at 11:41 UTC and radiosonde profile at 10:58 UTC.

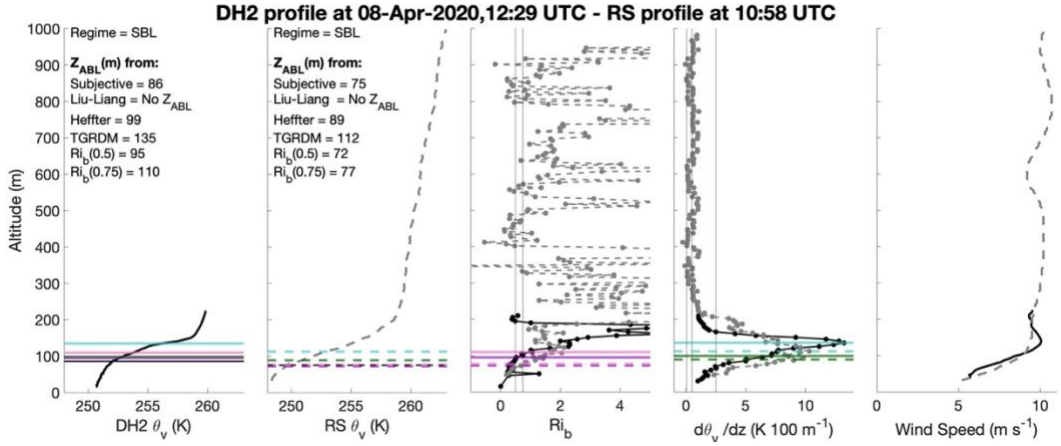

Figure S13: Z_{ABL} identification for DH2 flight on 8 April at 12:29 UTC and radiosonde profile at 10:58 UTC.

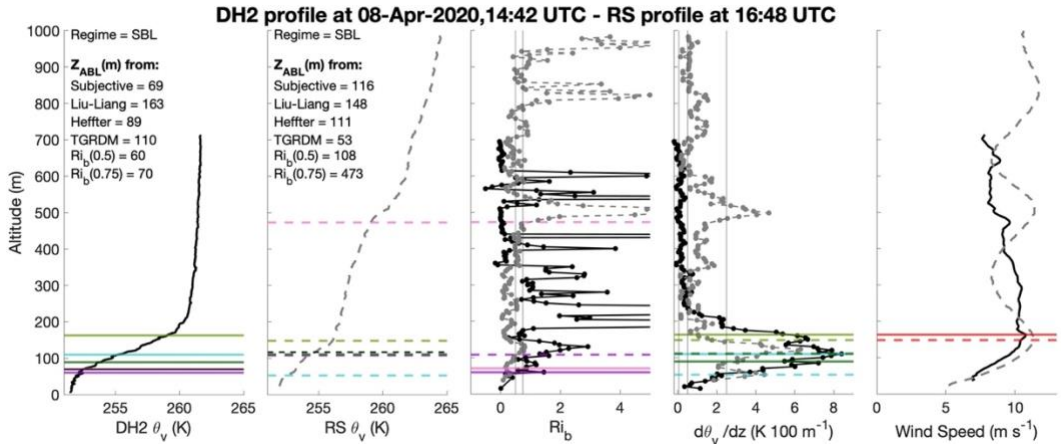

Figure S14: Z_{ABL} identification for DH2 flight on 8 April at 14:42 UTC and radiosonde profile at 16:48 UTC.

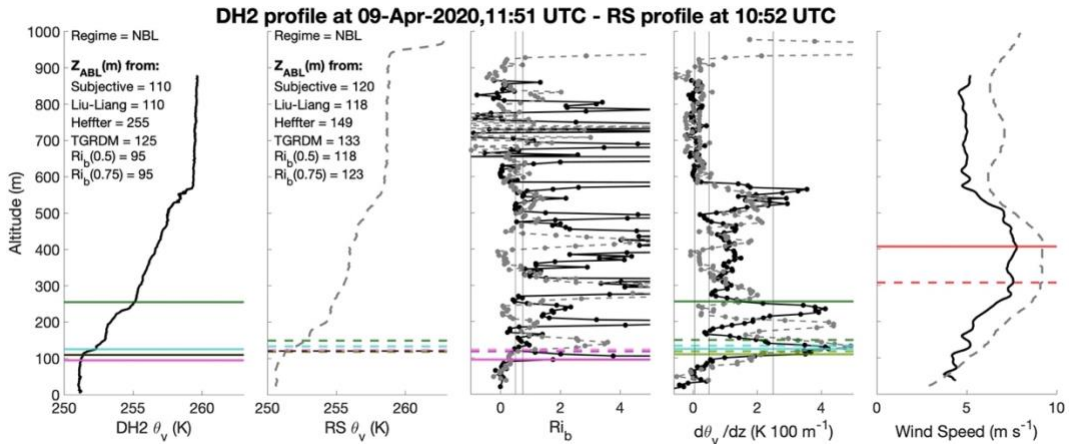

Figure S15: Z_{ABL} identification for DH2 flight on 9 April at 11:51 UTC and radiosonde profile at 10:52 UTC.

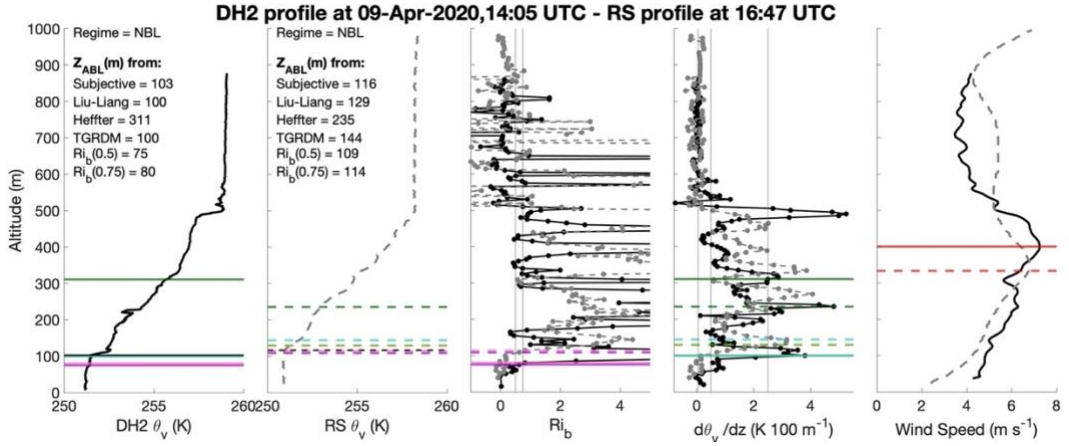

70

Figure S16: Z_{ABL} identification for DH2 flight on 9 April at 14:05 UTC and radiosonde profile at 16:47 UTC.

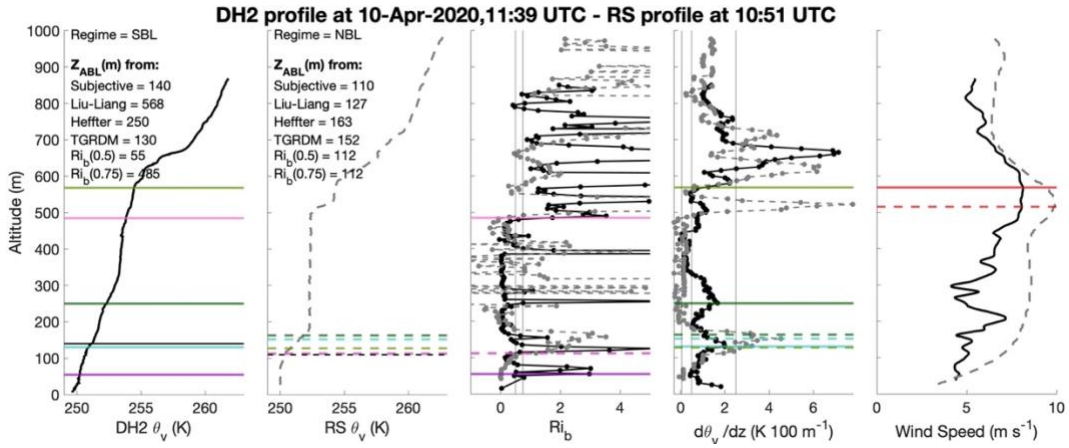

Figure S17: Z_{ABL} identification for DH2 flight on 10 April at 11:39 UTC and radiosonde profile at 10:51 UTC.

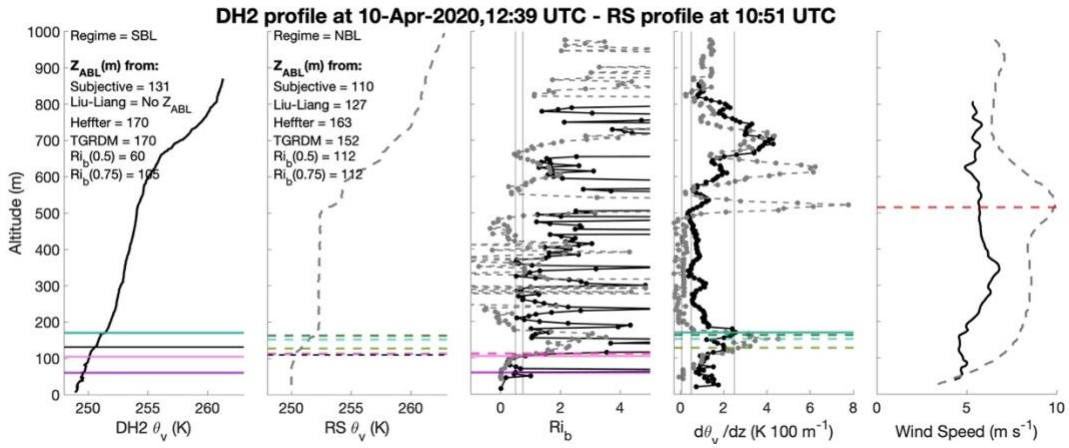

75 **Figure S18:** Z_{ABL} identification for DH2 flight on 10 April at 12:39 UTC and radiosonde profile at 10:51 UTC.

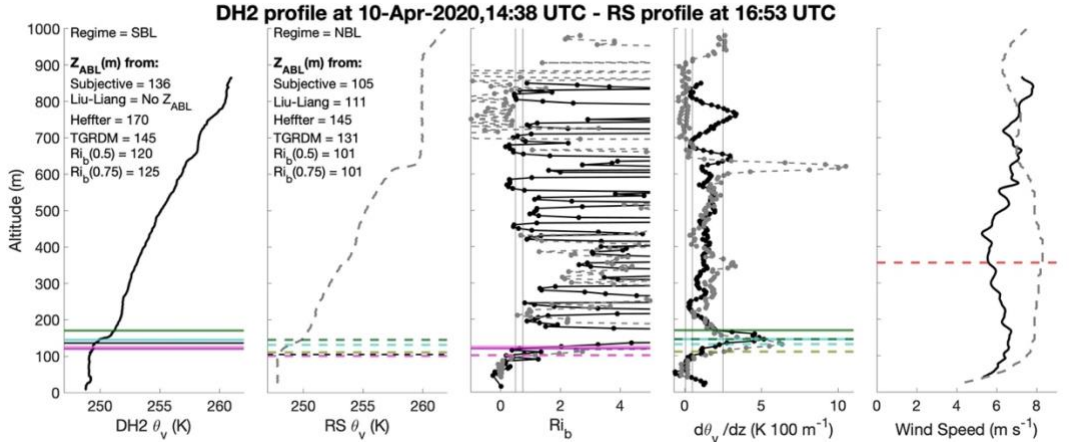

Figure S19: Z_{ABL} identification for DH2 flight on 10 April at 14:38 UTC and radiosonde profile at 16:53 UTC.

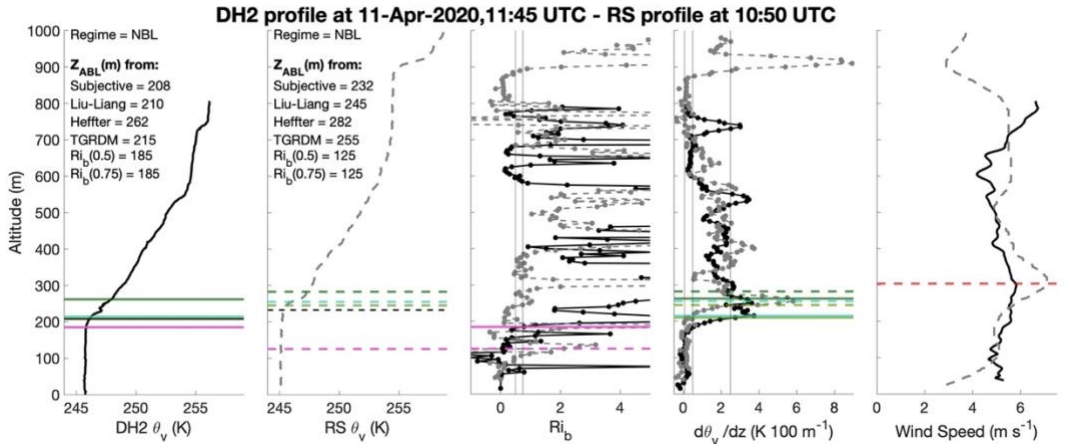

Figure S20: Z_{ABL} identification for DH2 flight on 11 April at 11:45 UTC and radiosonde profile at 10:50 UTC.

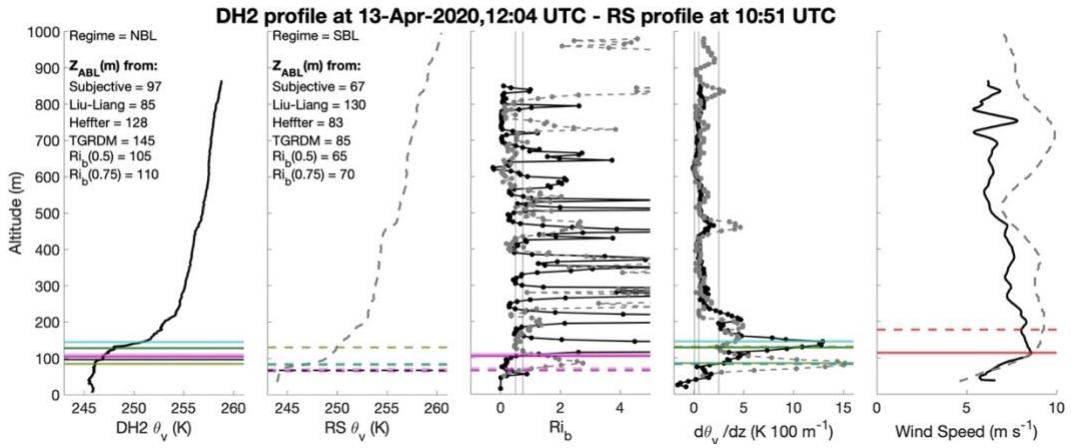

80

Figure S21: Z_{ABL} identification for DH2 flight on 13 April at 12:04 UTC and radiosonde profile at 10:51 UTC.

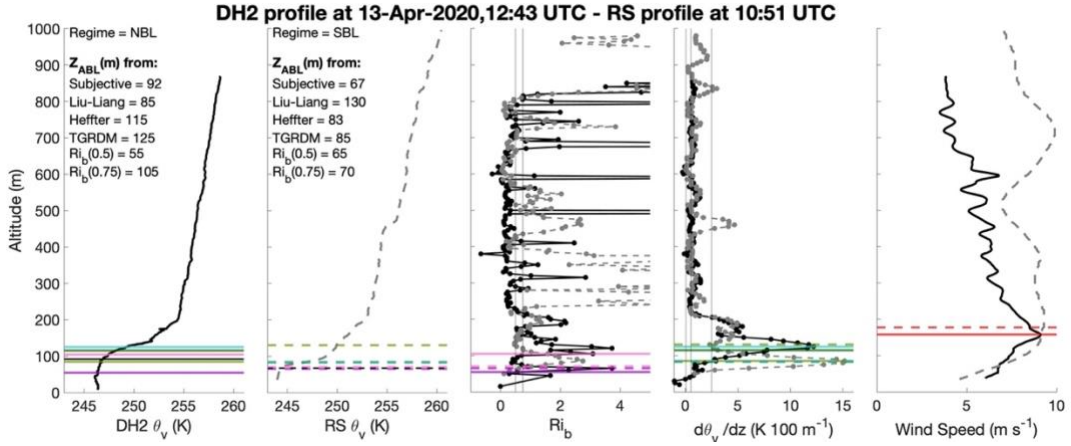

Figure S22: Z_{ABL} identification for DH2 flight on 13 April at 12:43 UTC and radiosonde profile at 10:51 UTC.

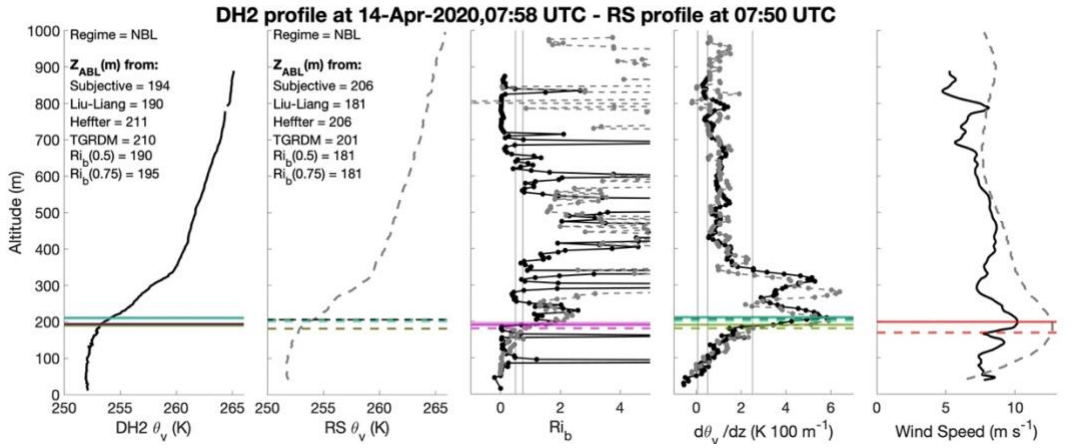

85 **Figure S23:** Z_{ABL} identification for DH2 flight on 14 April at 7:58 UTC and radiosonde profile at 7:50 UTC.

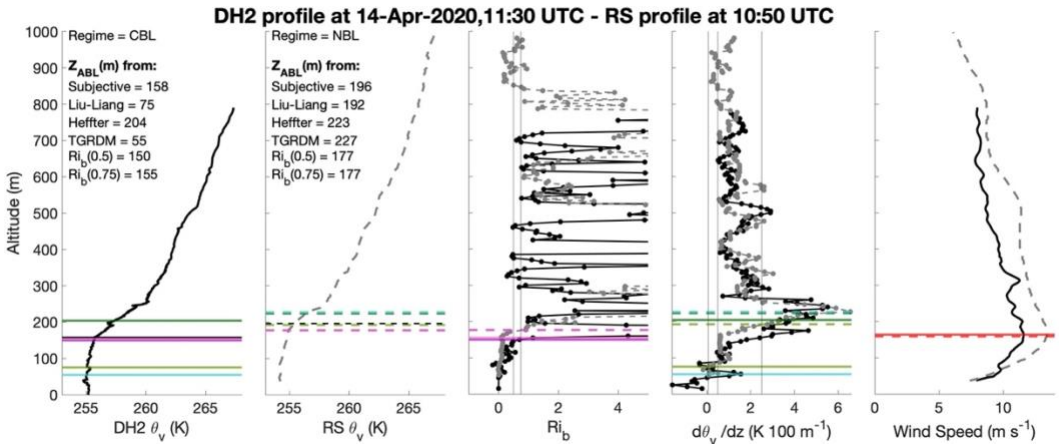

Figure S24: Z_{ABL} identification for DH2 flight on 14 April at 11:30 UTC and radiosonde profile at 10:50 UTC.

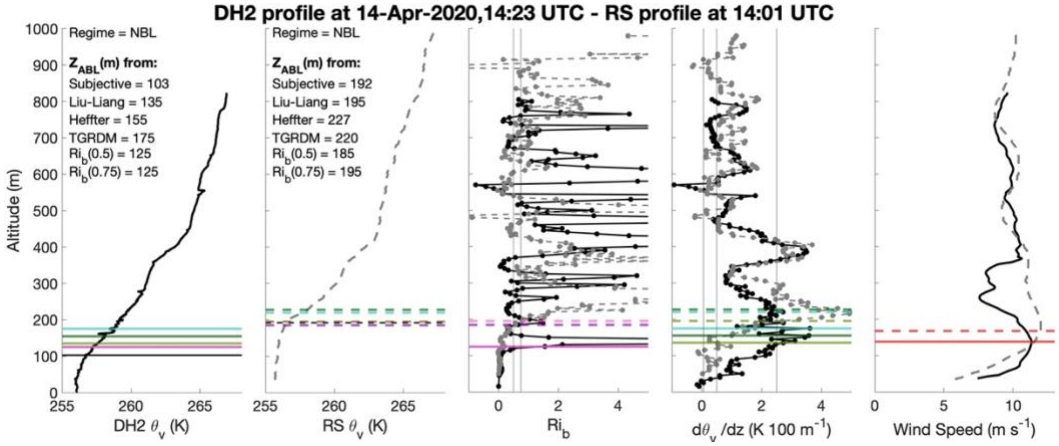

Figure S25: Z_{ABL} identification for DH2 flight on 14 April at 14:23 UTC and radiosonde profile at 14:01 UTC.

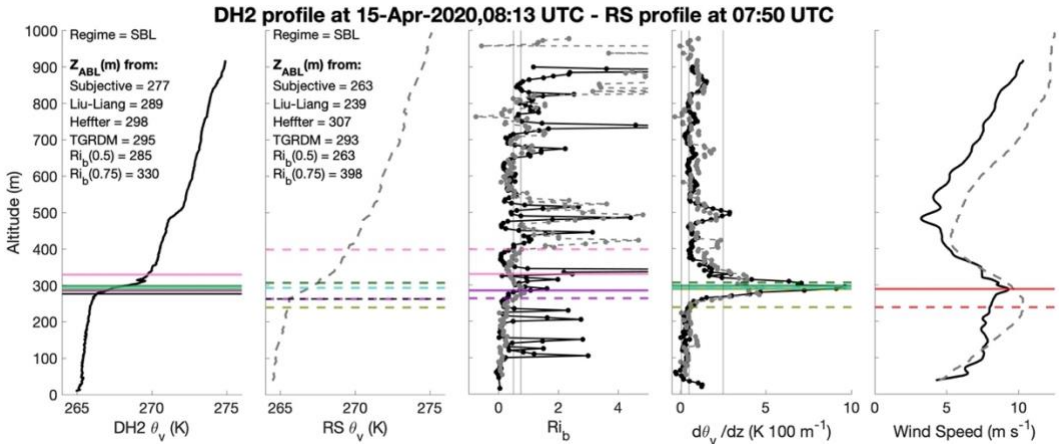

90

Figure S26: Z_{ABL} identification for DH2 flight on 15 April at 8:13 UTC and radiosonde profile at 7:50 UTC.

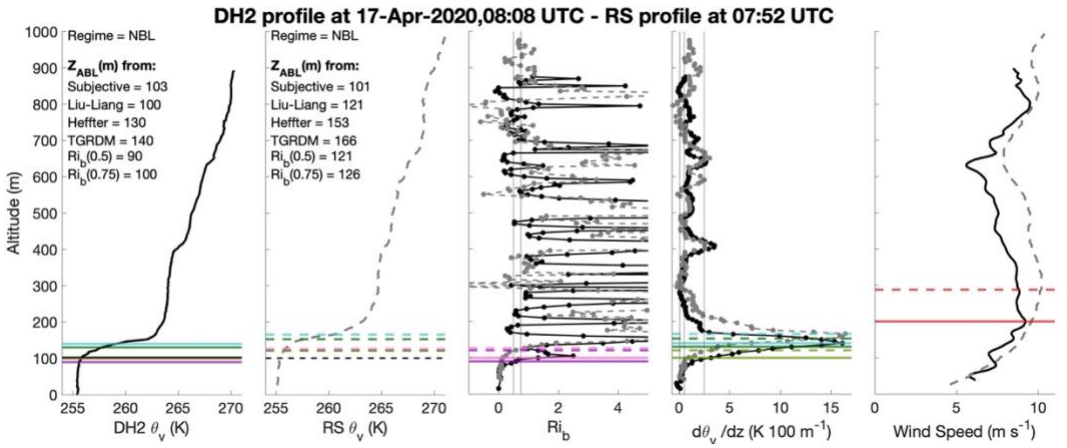

Figure S27: Z_{ABL} identification for DH2 flight on 17 April at 8:08 UTC and radiosonde profile at 7:52 UTC.

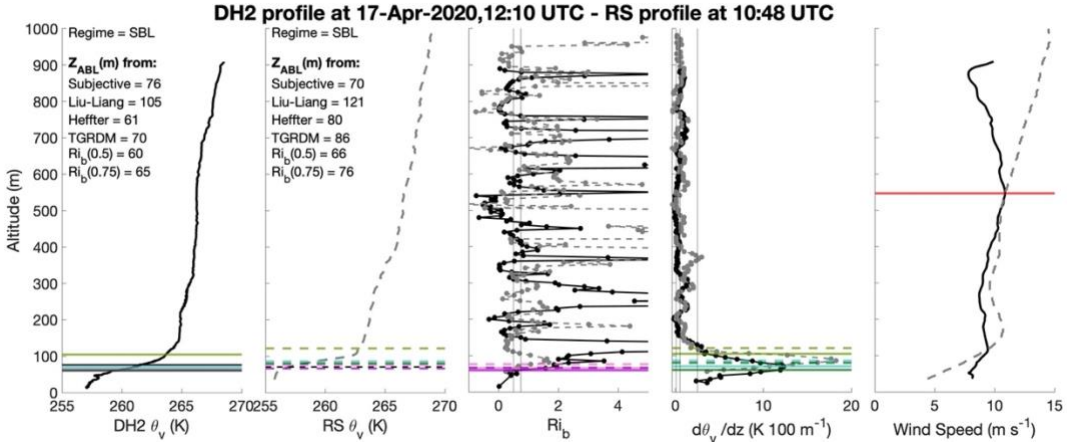

95 **Figure S28:** Z_{ABL} identification for DH2 flight on 17 April at 12:10 UTC and radiosonde profile at 10:48 UTC

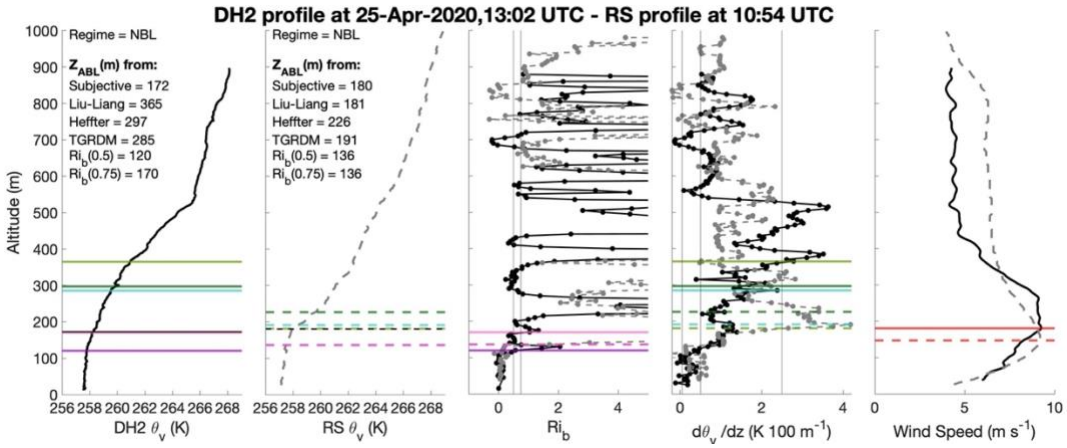

Figure S29: Z_{ABL} identification for DH2 flight on 25 April at 13:02 UTC and radiosonde profile at 10:54 UTC.

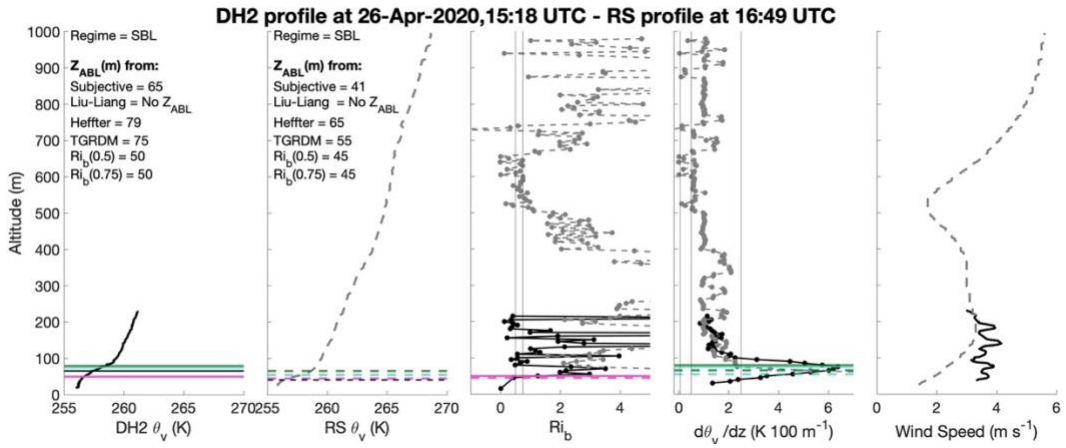

Figure S30: Z_{ABL} identification for DH2 flight on 26 April at 15:18 UTC and radiosonde profile at 16:49 UTC.

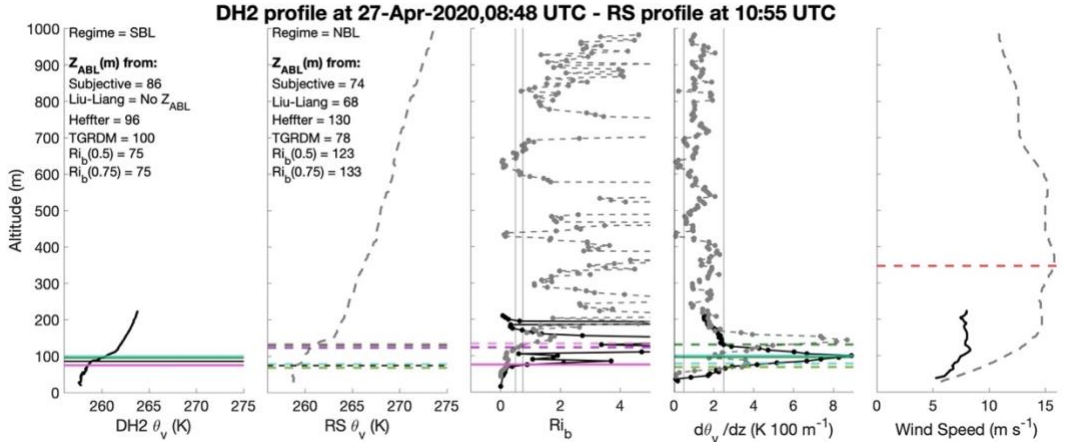

100

Figure S31: Z_{ABL} identification for DH2 flight on 27 April at 8:48 UTC and radiosonde profile at 10:55 UTC.

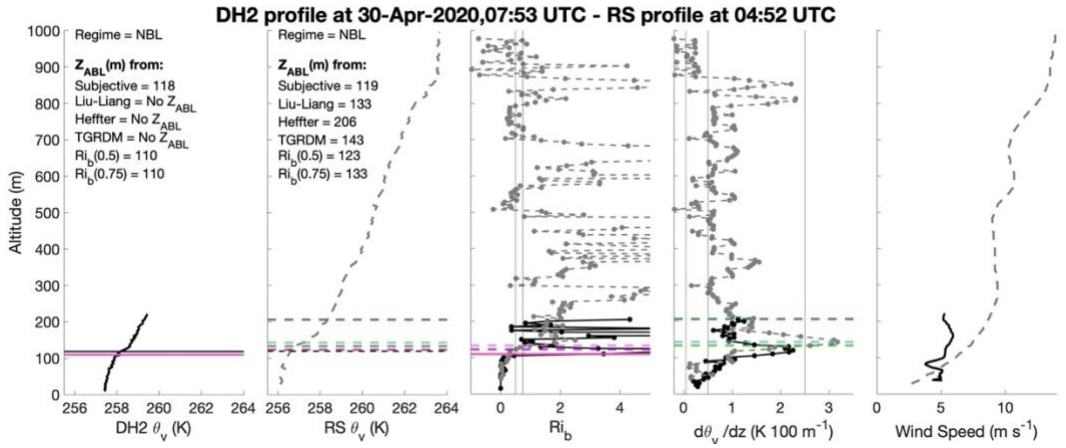

Figure S32: Z_{ABL} identification for DH2 flight on 30 April at 7:53 UTC and radiosonde profile at 4:52 UTC.

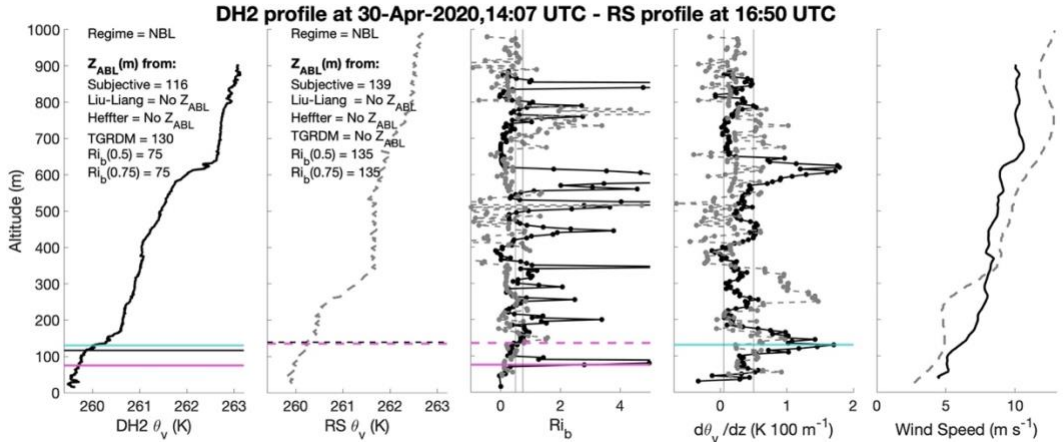

105 **Figure S33:** Z_{ABL} identification for DH2 flight on 30 April at 14:07 UTC and radiosonde profile at 16:50 UTC.

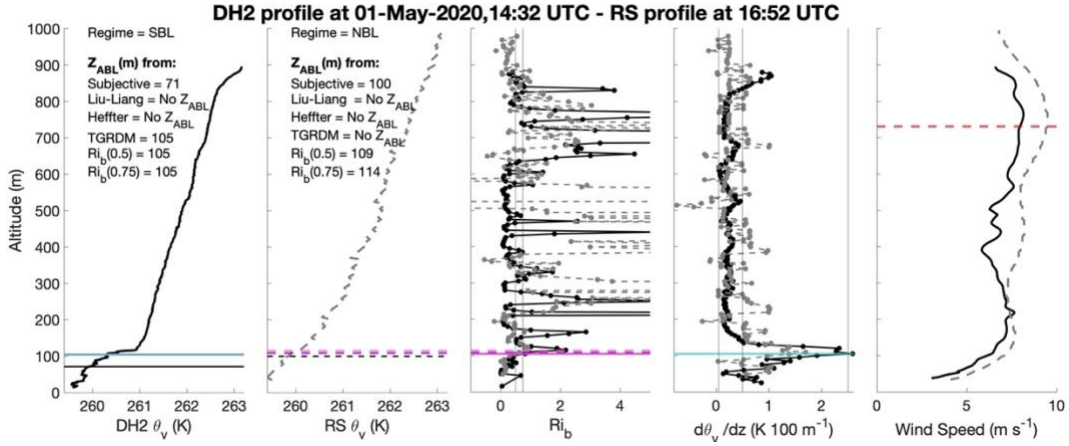

Figure S34: Z_{ABL} identification for DH2 flight on 1 May at 14:32 UTC and radiosonde profile at 16:52 UTC.

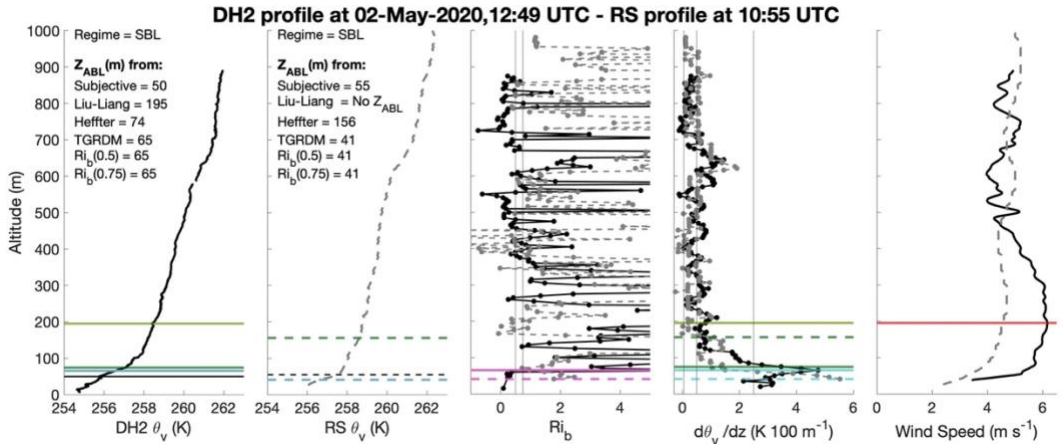

Figure S35: Z_{ABL} identification for DH2 flight on 2 May at 12:49 UTC and radiosonde profile at 10:55 UTC.

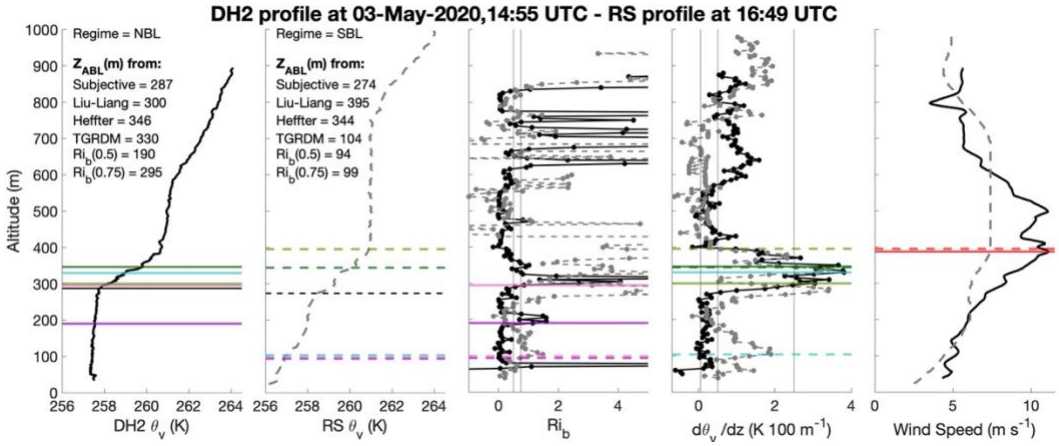

110

Figure S36: Z_{ABL} identification for DH2 flight on 3 May at 14:55 UTC and radiosonde profile at 16:49 UTC

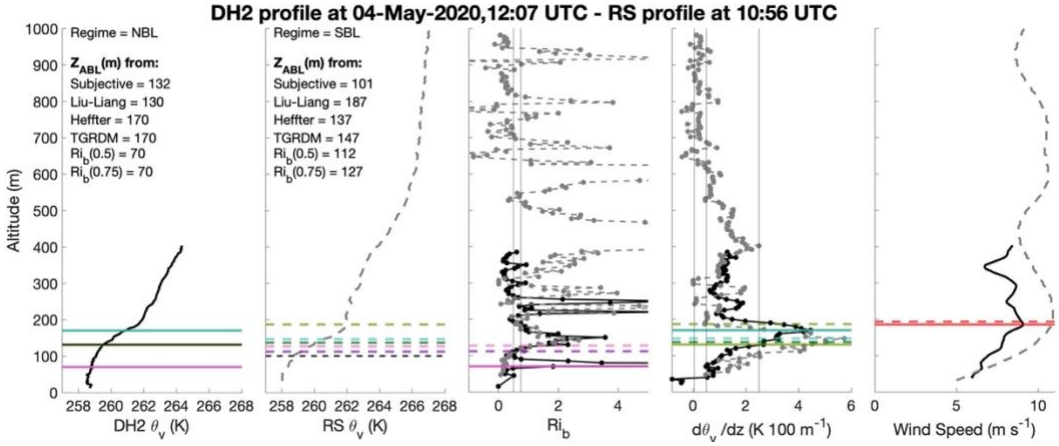

Figure S37: Z_{ABL} identification for DH2 flight on 4 May at 12:07 UTC and radiosonde profile at 10:56 UTC.

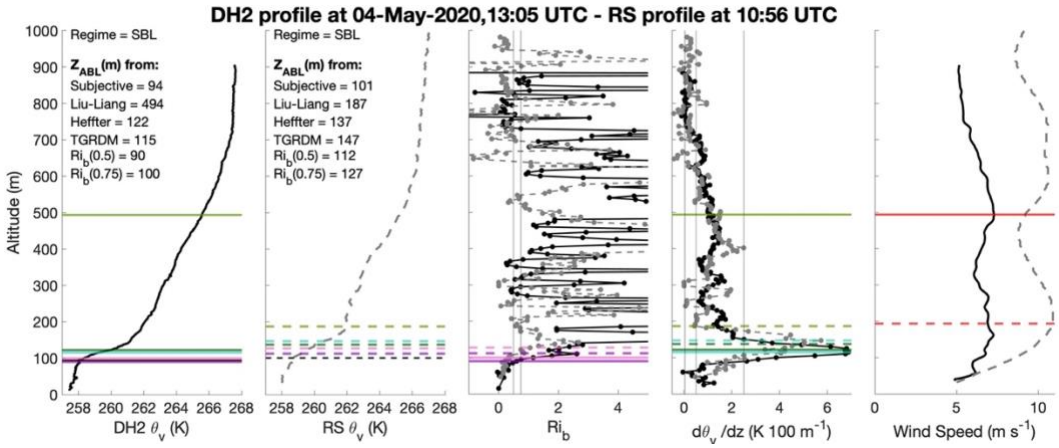

115 **Figure S38:** Z_{ABL} identification for DH2 flight on 4 May at 13:05 UTC and radiosonde profile at 10:56 UTC.

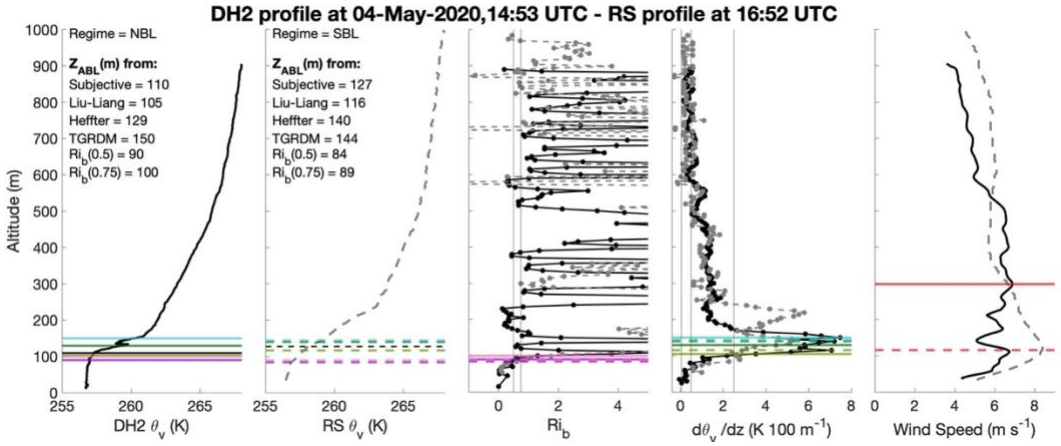

Figure S39: Z_{ABL} identification for DH2 flight on 4 May at 14:53 UTC and radiosonde profile at 16:52 UTC.

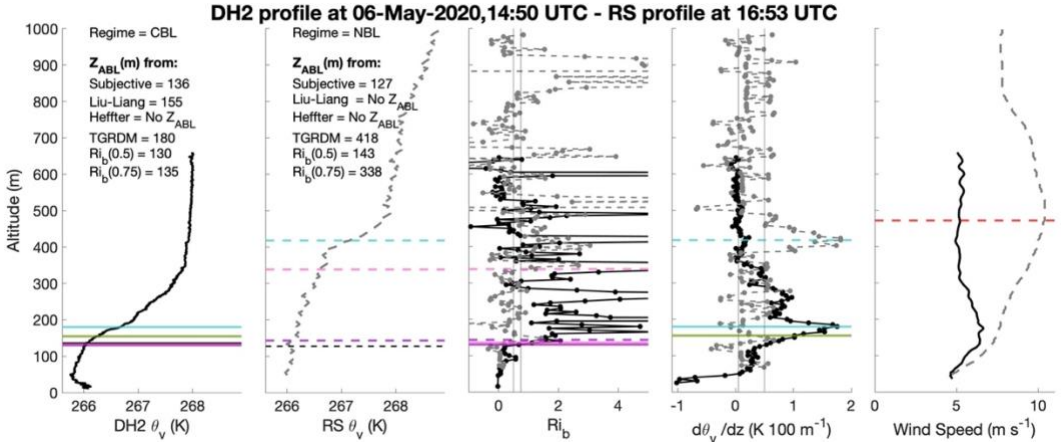

Figure S40: Z_{ABL} identification for DH2 flight on 6 May at 14:50 UTC and radiosonde profile at 16:53 UTC.

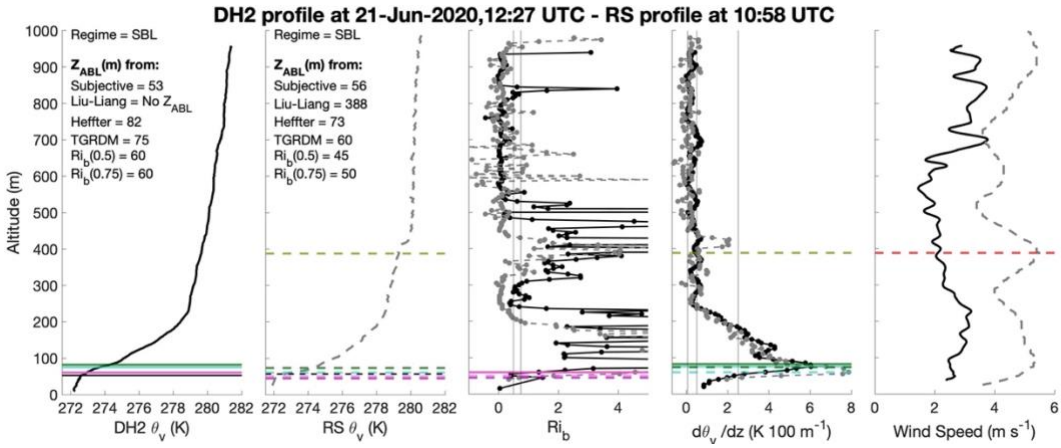

120

Figure S41: Z_{ABL} identification for DH2 flight on 21 June at 12:27 UTC and radiosonde profile at 10:58 UTC.

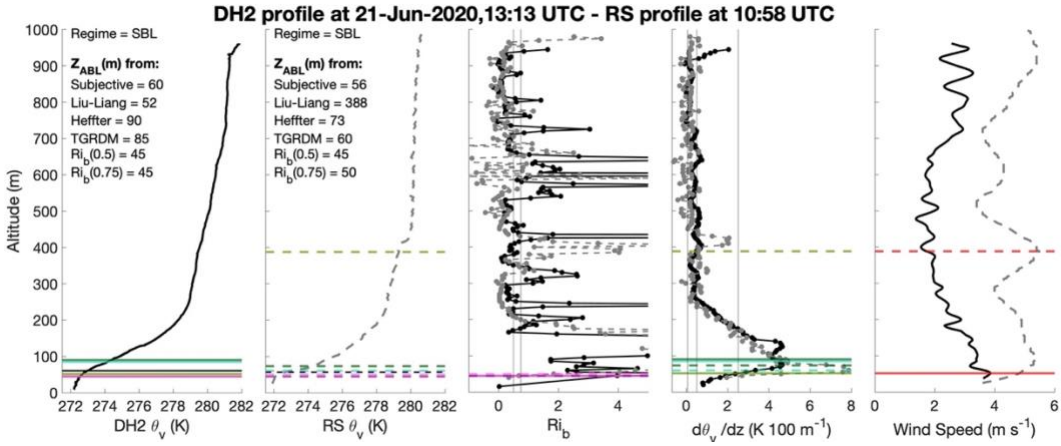

Figure S42: Z_{ABL} identification for DH2 flight on 21 June at 13:13 UTC and radiosonde profile at 10:58 UTC.

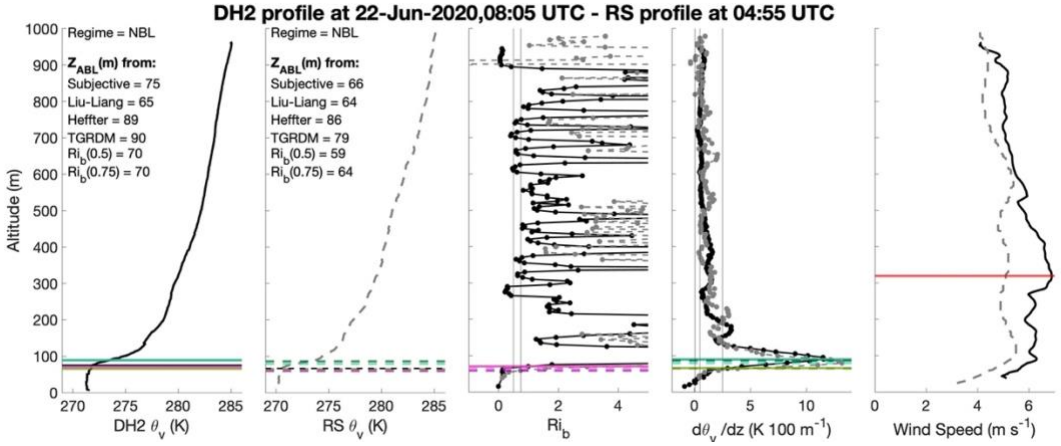

125 **Figure S43:** Z_{ABL} identification for DH2 flight on 22 June at 8:05 UTC and radiosonde profile at 4:55 UTC.

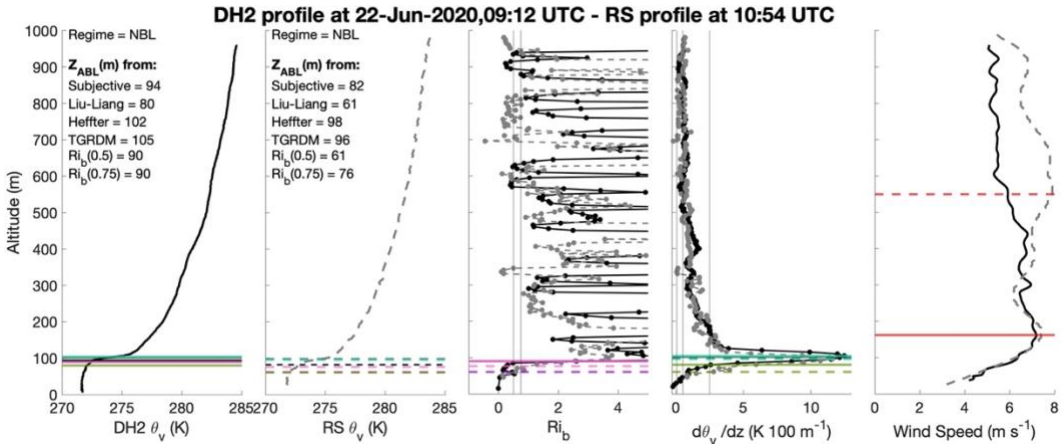

Figure S44: Z_{ABL} identification for DH2 flight on 22 June at 9:12 UTC and radiosonde profile at 10:54 UTC.

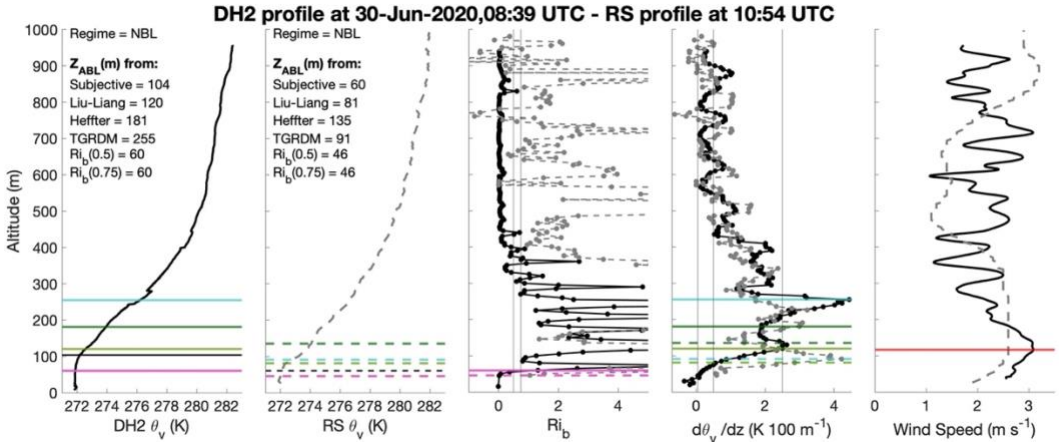

Figure S45: Z_{ABL} identification for DH2 flight on 30 June at 8:39 UTC and radiosonde profile at 10:54 UTC.

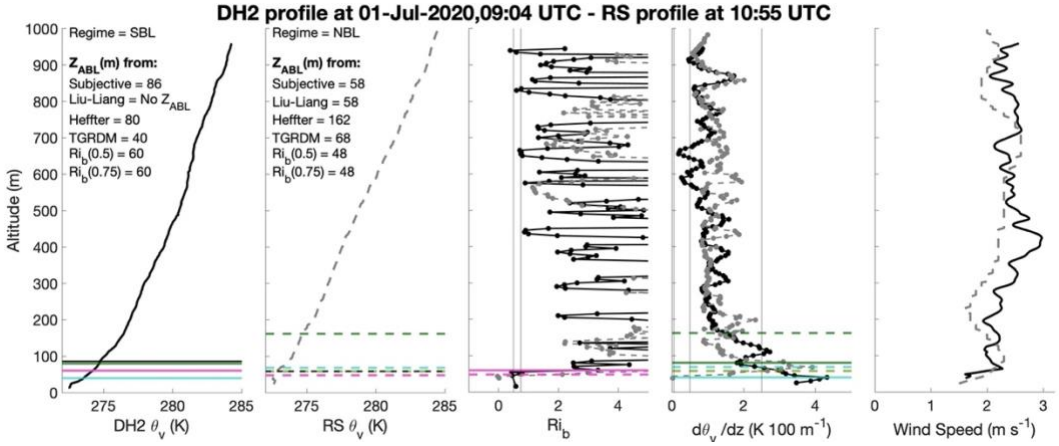

130

Figure S46: Z_{ABL} identification for DH2 flight on 1 July at 9:04 UTC and radiosonde profile at 10:55 UTC.

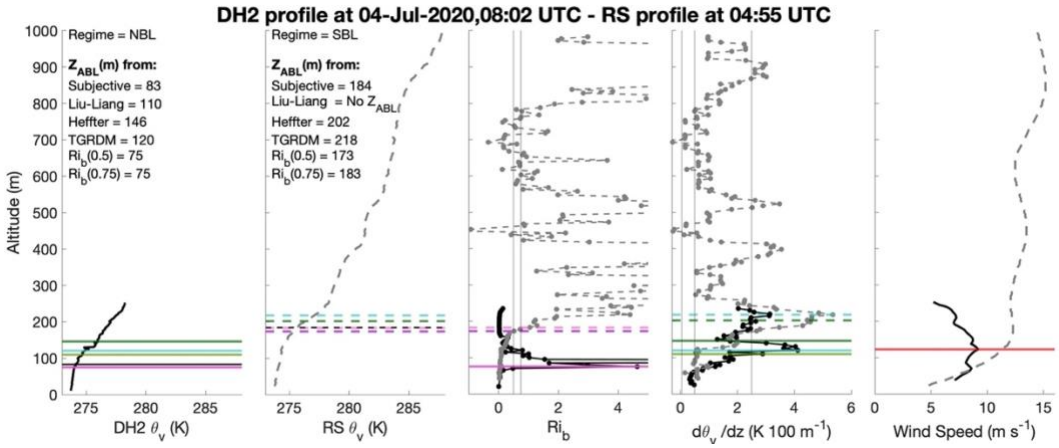

Figure S47: Z_{ABL} identification for DH2 flight on 4 July at 8:02 UTC and radiosonde profile at 4:55 UTC

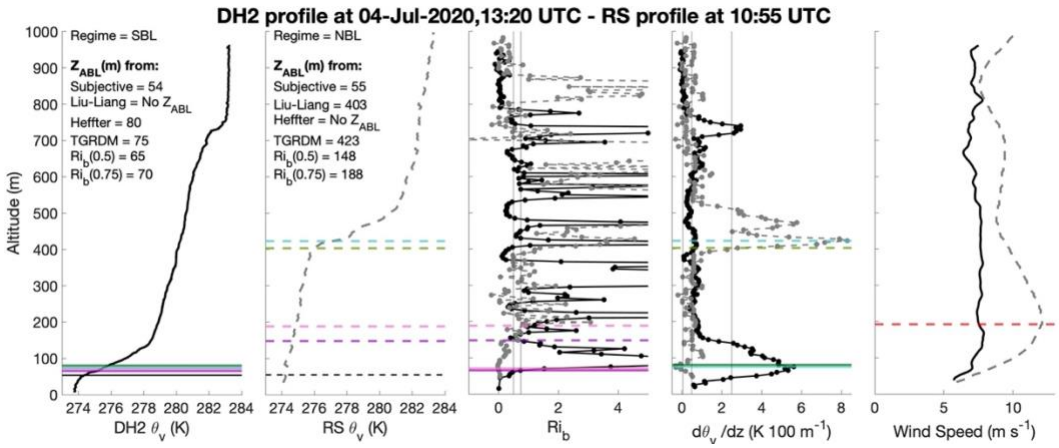

135 **Figure S48:** Z_{ABL} identification for DH2 flight on 4 July at 13:20 UTC and radiosonde profile at 10:55 UTC.

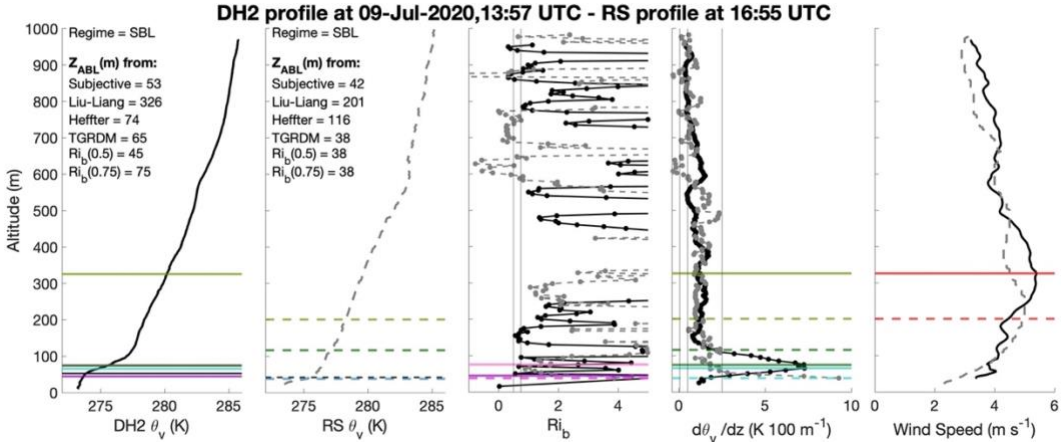

Figure S49: Z_{ABL} identification for DH2 flight on 9 July at 13:57 UTC and radiosonde profile at 16:55 UTC.

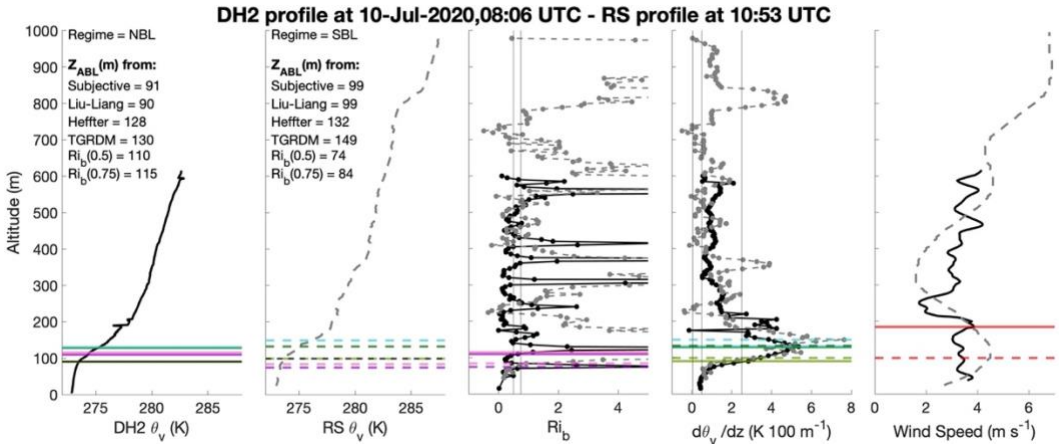

Figure S50: Z_{ABL} identification for DH2 flight on 10 July at 8:06 UTC and radiosonde profile at 10:53 UTC.

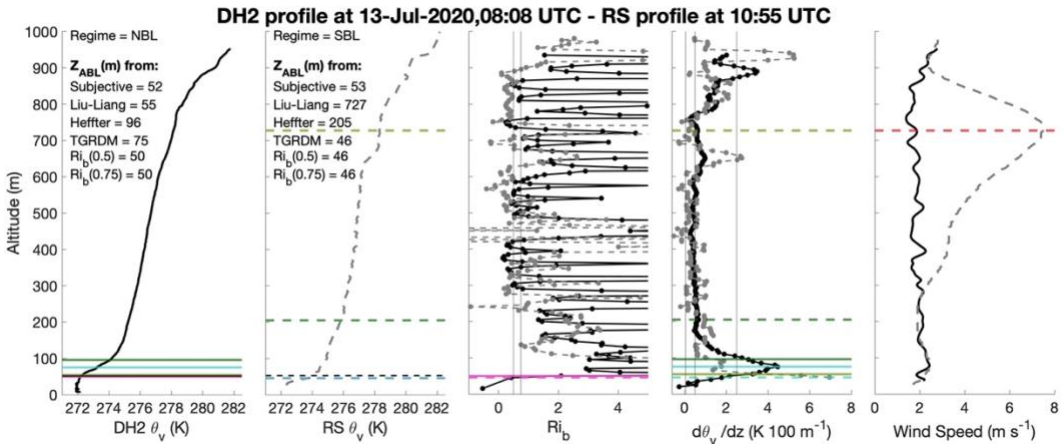

140

Figure S51: Z_{ABL} identification for DH2 flight on 13 July at 8:08 UTC and radiosonde profile at 10:55 UTC.

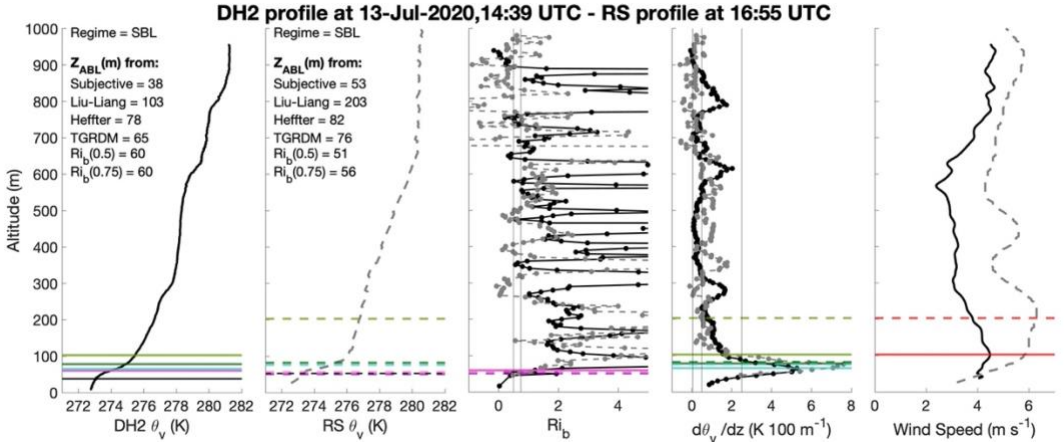

Figure S52: Z_{ABL} identification for DH2 flight on 13 July at 14:39 UTC and radiosonde profile at 16:55 UTC.

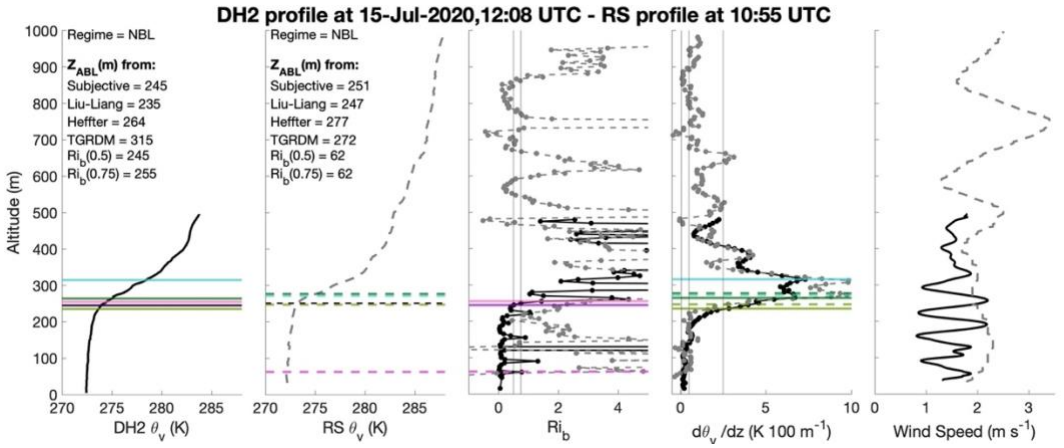

145 **Figure S53:** Z_{ABL} identification for DH2 flight on 15 July at 12:08 UTC and radiosonde profile at 10:55 UTC.

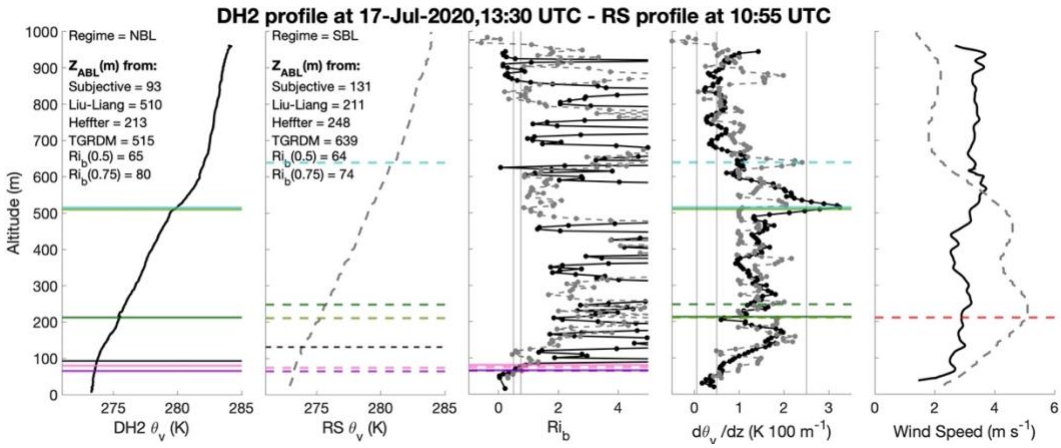

Figure S54: Z_{ABL} identification for DH2 flight on 17 July at 13:30 UTC and radiosonde profile at 10:55 UTC.

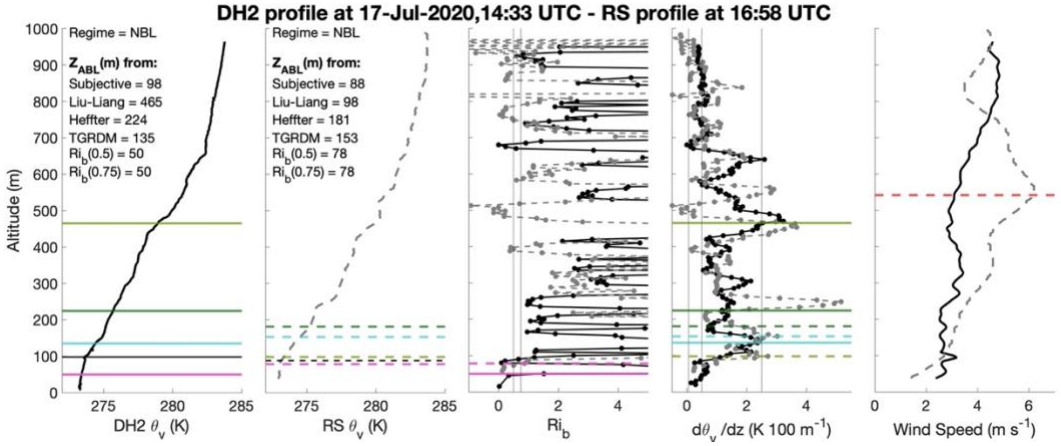

Figure S55: Z_{ABL} identification for DH2 flight on 17 July at 14:33 UTC and radiosonde profile at 16:58 UTC.

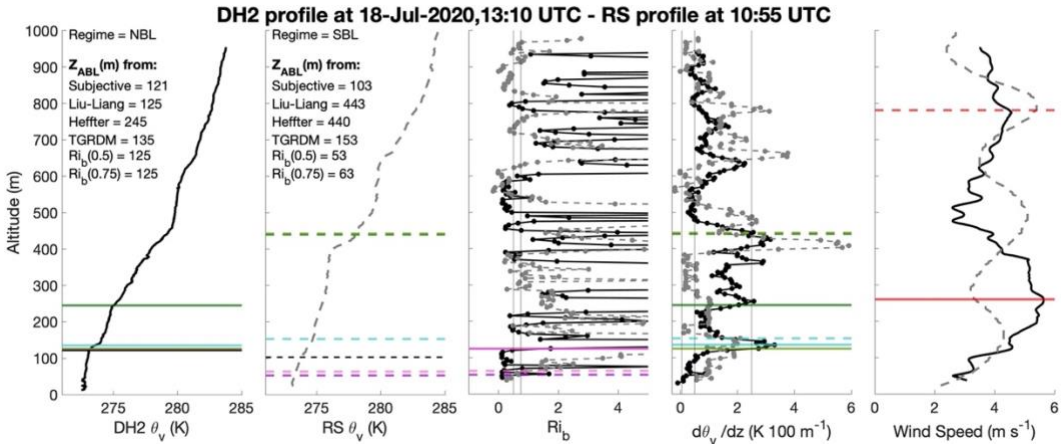

Figure S56: Z_{ABL} identification for DH2 flight on 18 July at 13:10 UTC and radiosonde profile at 10:55 UTC.

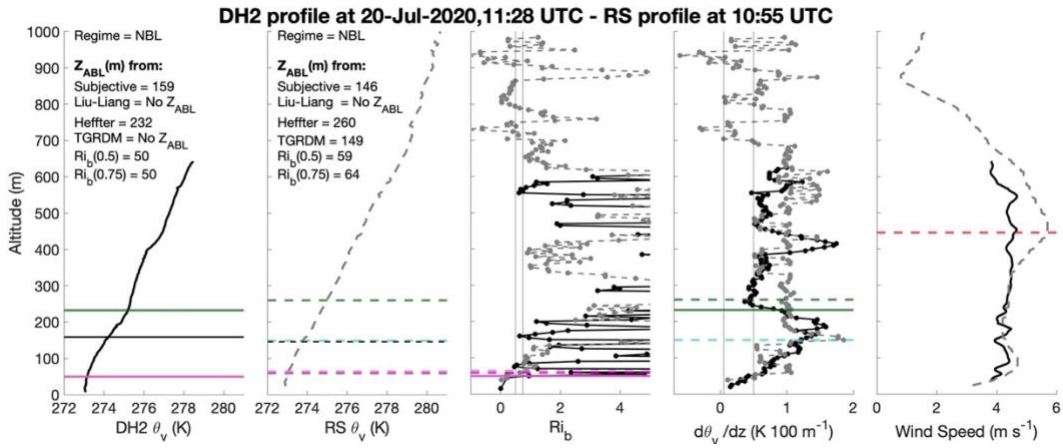

Figure S57: Z_{ABL} identification for DH2 flight on 20 July at 11:28 UTC and radiosonde profile at 10:55 UTC.

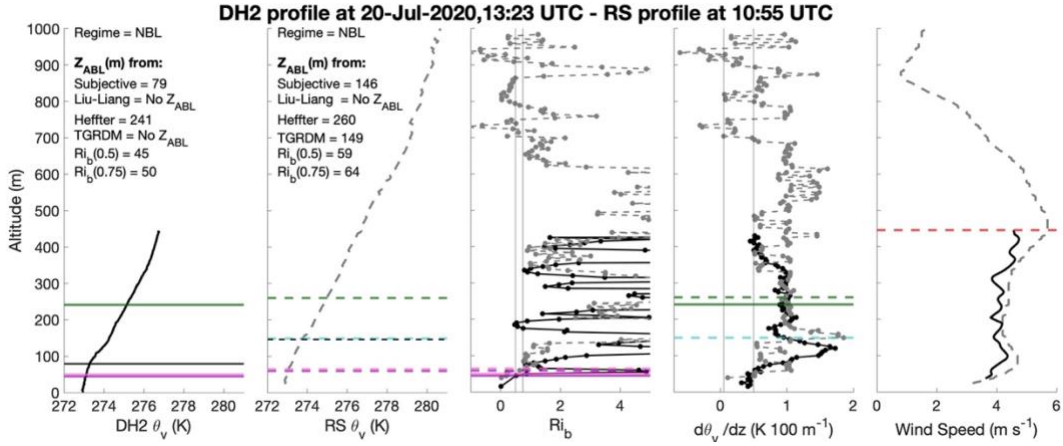

155 **Figure S58:** Z_{ABL} identification for DH2 flight on 20 July at 13:23 UTC and radiosonde profile at 10:55 UTC.

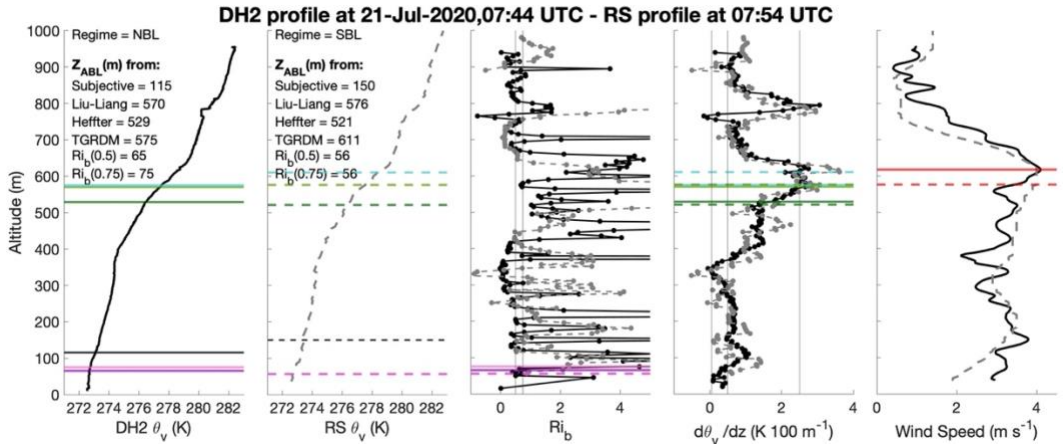

Figure S59: Z_{ABL} identification for DH2 flight on 21 July at 7:44 UTC and radiosonde profile at 7:54 UTC.

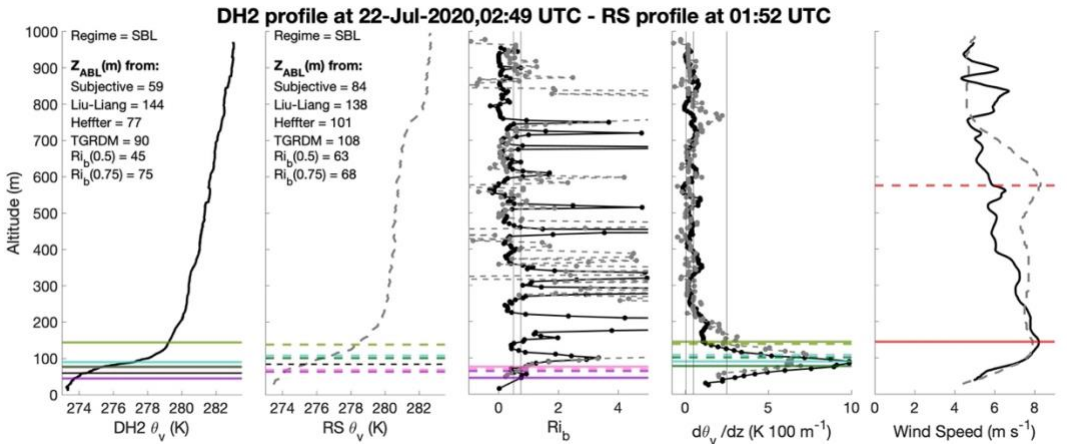

Figure S60: Z_{ABL} identification for DH2 flight on 22 July at 2:49 UTC and radiosonde profile at 1:52 UTC.

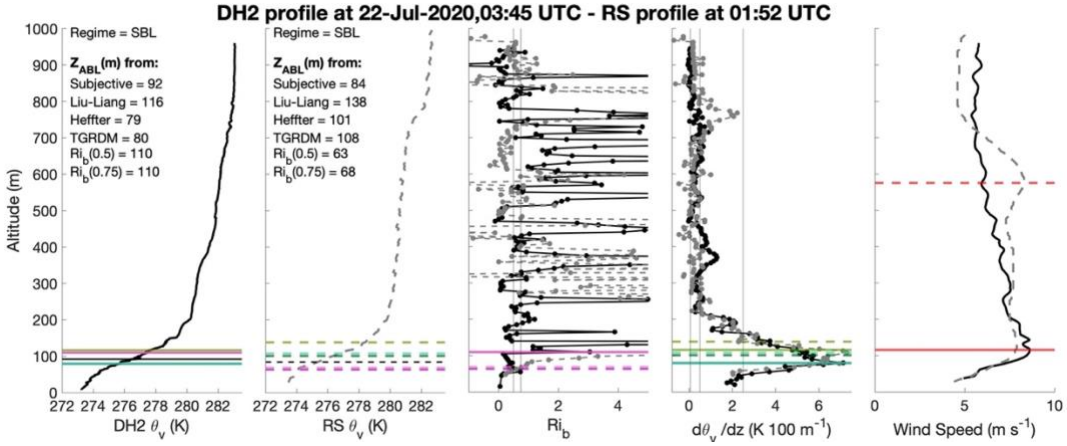

160

Figure S61: Z_{ABL} identification for DH2 flight on 22 July at 3:45 UTC and radiosonde profile at 1:52 UTC.

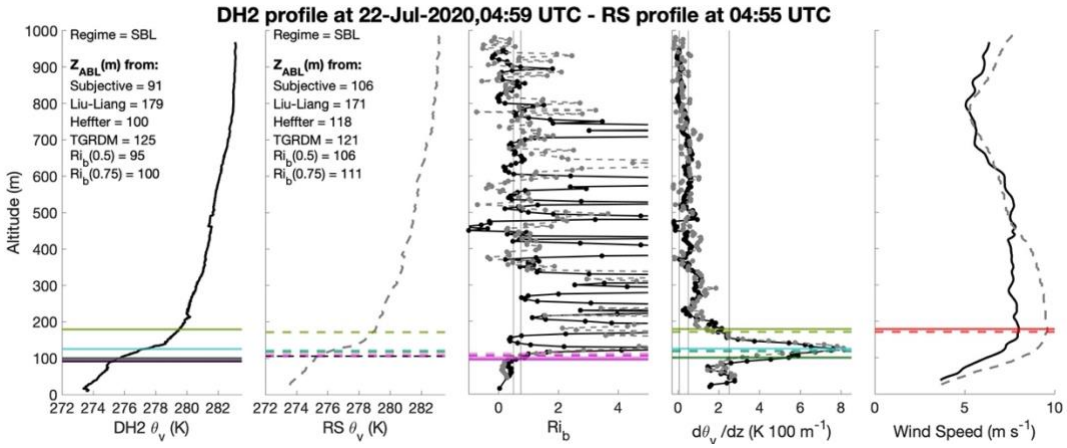

Figure S62: Z_{ABL} identification for DH2 flight on 22 July at 4:59 UTC and radiosonde profile at 4:55 UTC.

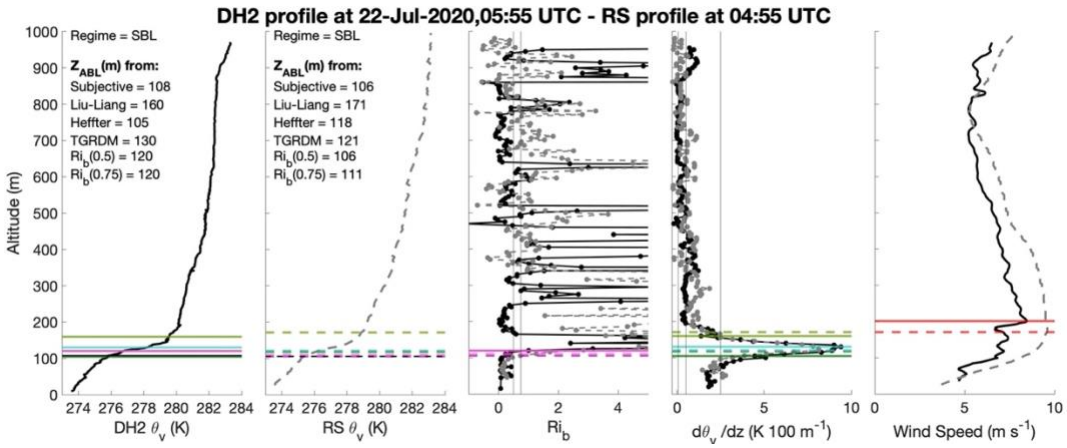

165 **Figure S63:** Z_{ABL} identification for DH2 flight on 22 July at 5:55 UTC and radiosonde profile at 4:55 UTC.

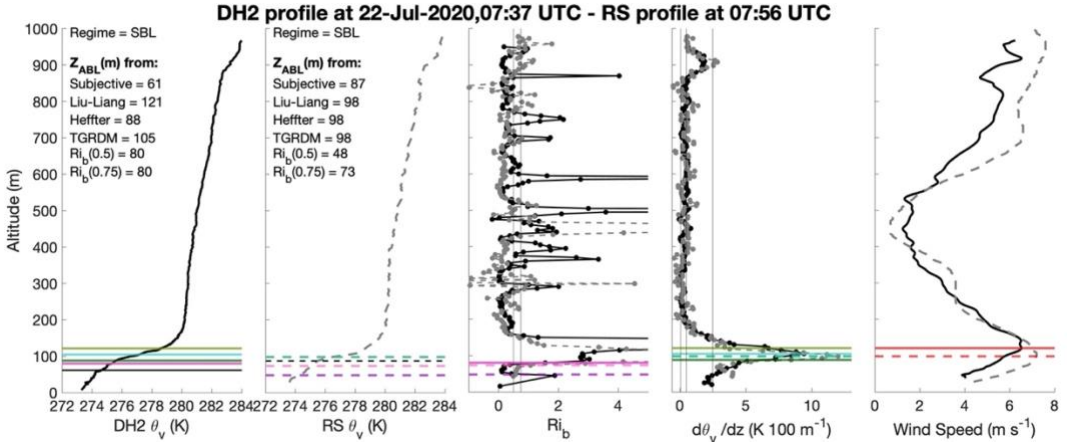

Figure S64: Z_{ABL} identification for DH2 flight on 22 July at 7:37 UTC and radiosonde profile at 7:56 UTC.

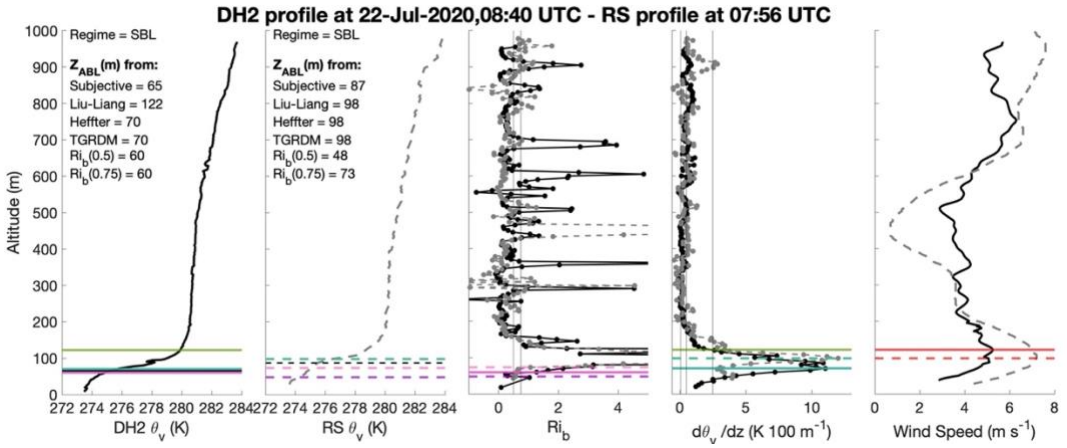

Figure S65: Z_{ABL} identification for DH2 flight on 22 July at 8:40 UTC and radiosonde profile at 7:56 UTC.

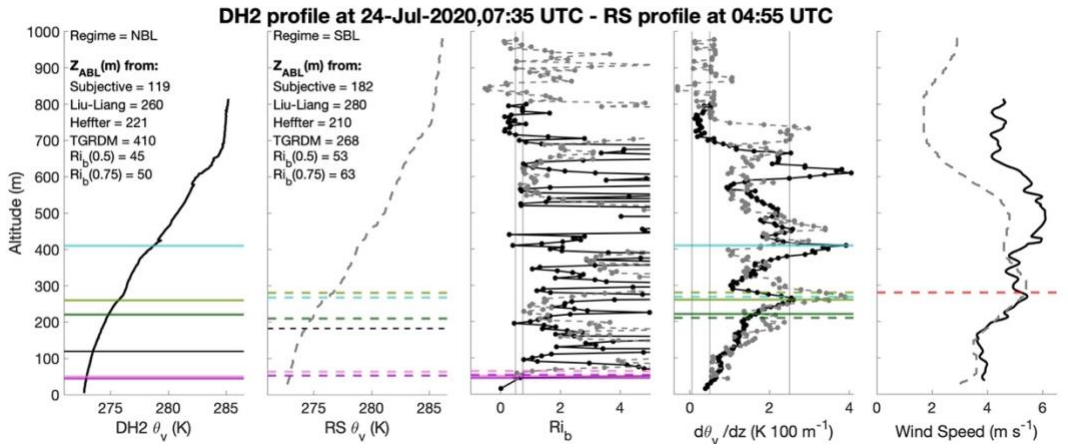

170

Figure S66: Z_{ABL} identification for DH2 flight on 24 July at 7:35 UTC and radiosonde profile at 4:55 UTC.

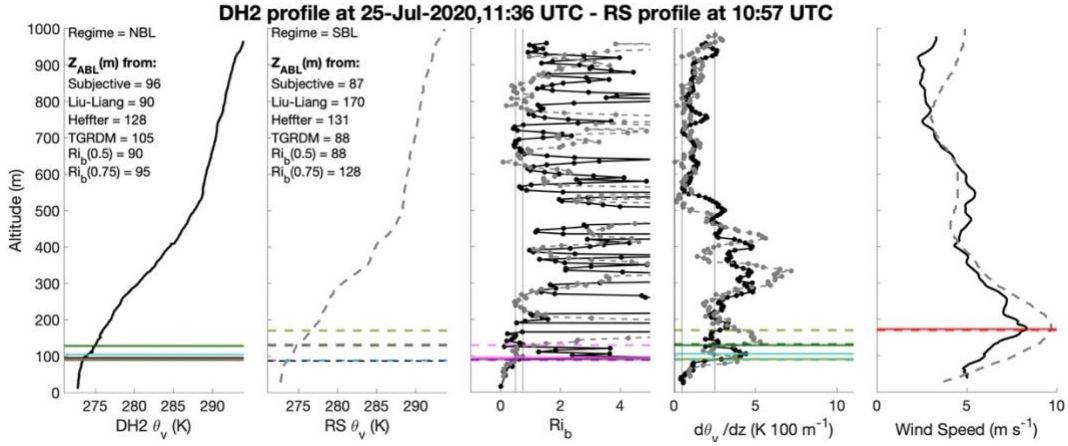

Figure S67: Z_{ABL} identification for DH2 flight on 25 July at 11:36 UTC and radiosonde profile at 10:57 UTC.

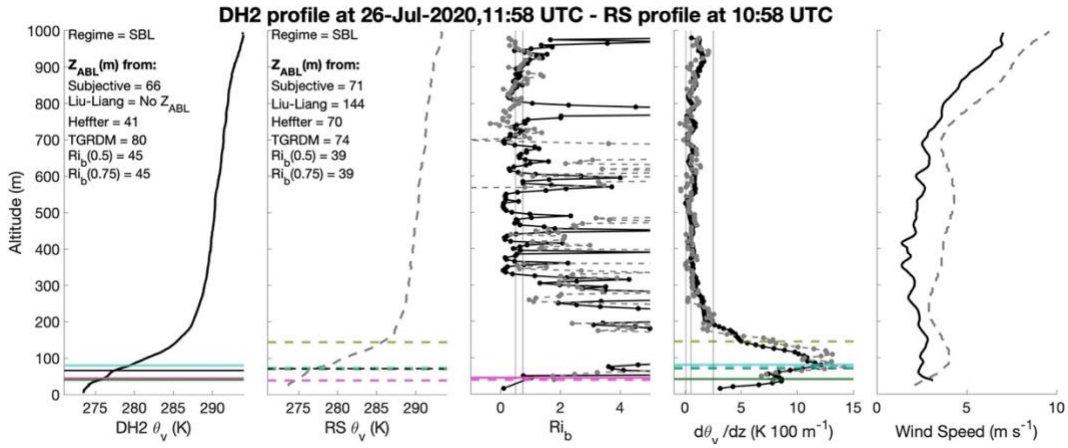

175 **Figure S68:** Z_{ABL} identification for DH2 flight on 26 July at 11:58 UTC and radiosonde profile at 10:58 UTC.

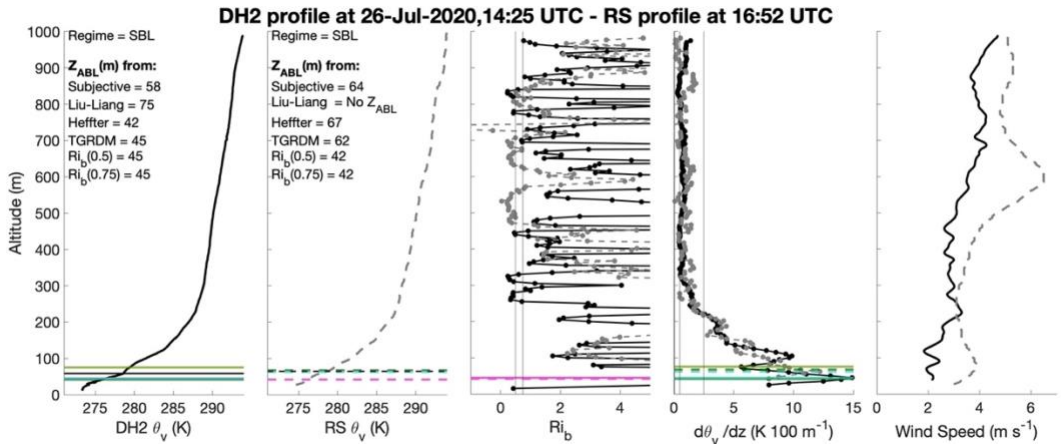

Figure S69: Z_{ABL} identification for DH2 flight on 26 July at 14:25 UTC and radiosonde profile at 16:52 UTC.

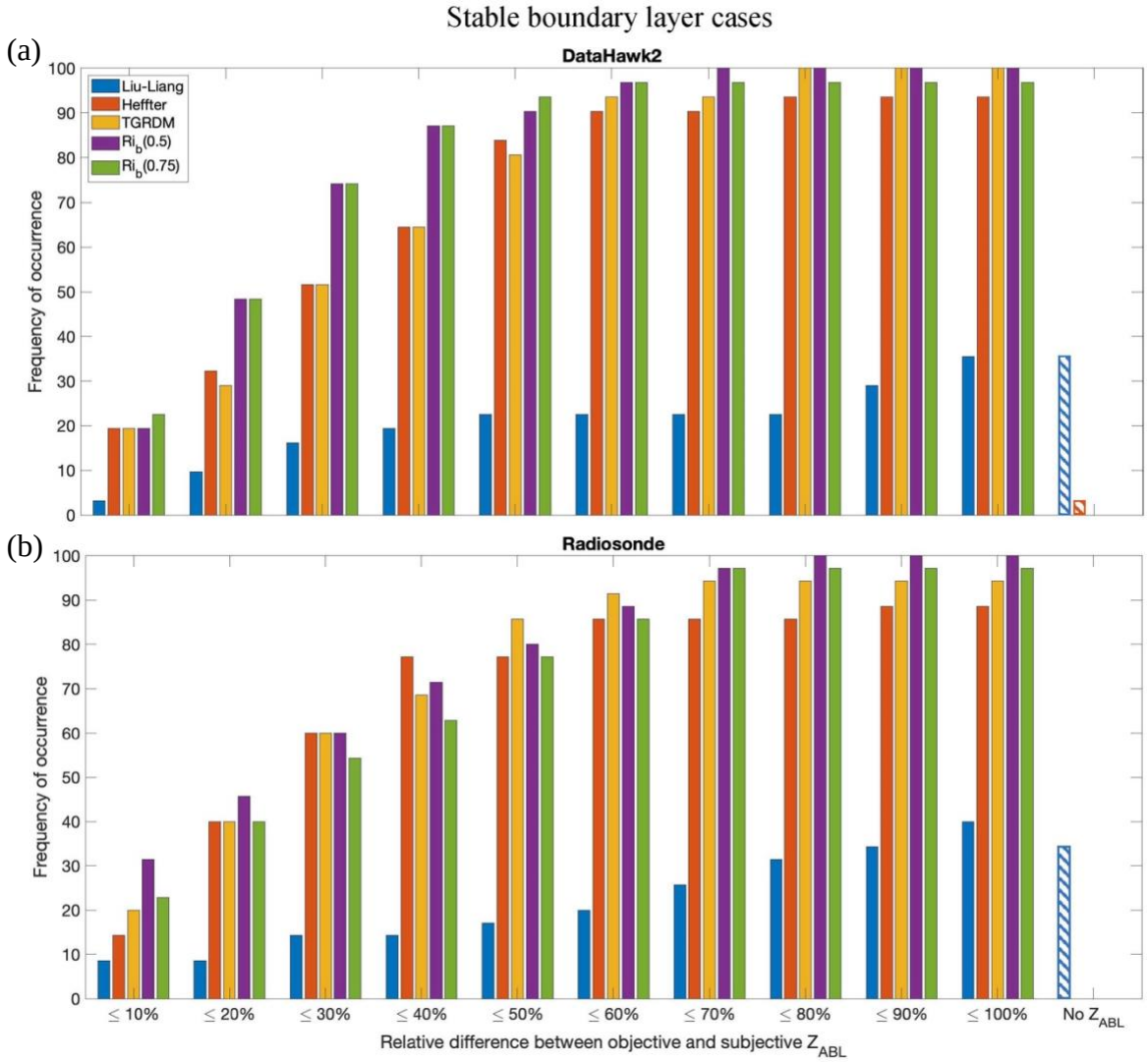

180 **Figure S70:** Bar plot showing what percent of **(a)** DH2 cases and **(b)** radiosonde cases give an objective Z_{ABL} within different relative difference ranges from the subjective Z_{ABL} using the different objective methods, for only stable cases. Plot also shows the percent of cases for each method where no Z_{ABL} is found (labelled as "No Z_{ABL}").

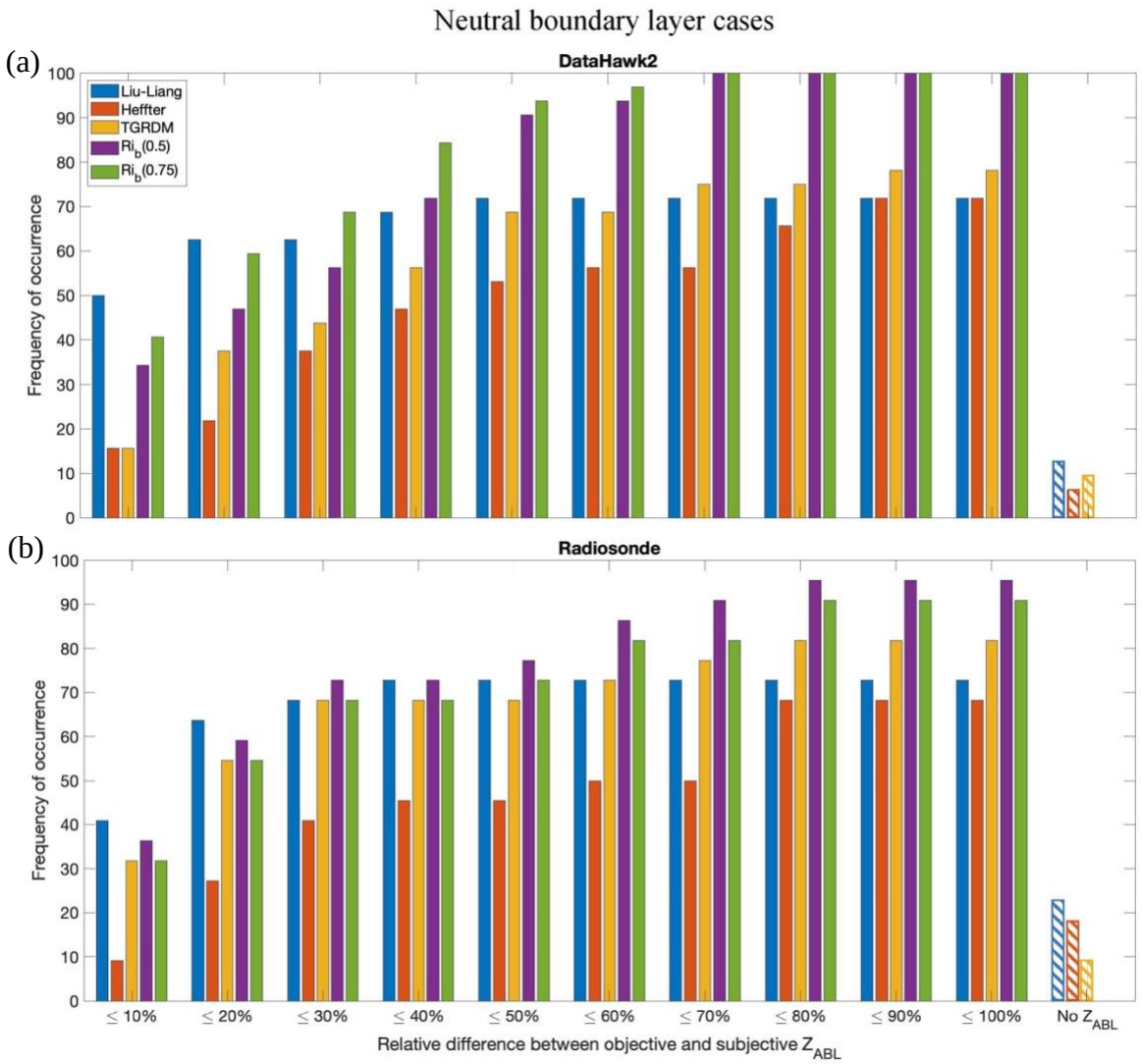

185 **Figure S71:** Bar plot showing what percent of **(a)** DH2 cases and **(b)** radiosonde cases give an objective Z_{ABL} within different relative difference ranges from the subjective Z_{ABL} using the different objective methods, for only neutral cases. Plot also shows the percent of cases for each method where no Z_{ABL} is found (labelled as "No Z_{ABL}").